

FLUKA cross sections for cosmic-ray interactions with the DRAGON2 code

P. De La Torre Luque,^{a,*} M.N. Mazziotta,^{b,*} A. Ferrari,^c
F. Loparco,^{b,d} P.R. Sala^e and D. Serini^b

^aThe Oskar Klein Centre, Department of Physics, Stockholm University, AlbaNova, SE-10691 Stockholm, Sweden

^bIstituto Nazionale di Fisica Nucleare, Sezione di Bari, via Orabona 4, I-70126 Bari, Italy

^cInstitute of Astroparticle Physics, Karlsruhe Institute of Technology, Campus North, Bldg. 401, Postfach 3640, D-76021 Karlsruhe, Germany

^dDipartimento di Fisica “M. Merlin” dell’Università e del Politecnico di Bari, via Amendola 173, I-70126 Bari, Italy

^eIstituto Nazionale di Fisica Nucleare, Sezione di Milano, Via Celoria 16, 20133 Milano, Italy
E-mail: pedro.delatorreluque@fysik.su.se, mazziotta@ba.infn.it,
alfredo.ferrari@mi.infn.it, Francesco.Loparco@ba.infn.it, paola.sala@mi.infn.it,
[Davide.Serini@ba.infn.it](mailto: Davide.Serini@ba.infn.it)

Received February 11, 2022

Revised April 21, 2022

Accepted May 25, 2022

Published July 5, 2022

Abstract. Secondary particles produced in spallation reactions of cosmic rays with the interstellar gas provide valuable information that allow us to investigate the injection and transport of charged particles in the Galaxy. A good understanding of the cross sections of production of these particles is crucial to correctly interpret our models, although the existing experimental data is very scarce and uncertain. We have developed a new set of cross sections, both inelastic and inclusive, computed with the FLUKA Monte Carlo nuclear code and tested its compatibility with CR data. Inelastic and inclusive cross sections have been compared to the most up-to-date data and parameterisations finding a general good agreement.

Then, these cross sections have been implemented in the DRAGON2 code to characterize the spectra of CR nuclei up to $Z = 26$ and the secondary-to-primary ratios of B, Be and Li. Interestingly, we find that the FLUKA cross sections allow us to predict an energy-dependence of the B, Be and Li flux ratios which is compatible with AMS-02 data and to reproduce simultaneously these flux ratios with a scaling lower than 20%. Finally, we implement the cross sections of production of gamma rays, calculated with FLUKA, in the Gammasky code and compute diffuse gamma-ray sky maps and the local HI emissivity spectrum, finding a very good agreement with Fermi Large Area Telescope data.

Keywords: cosmic ray experiments, cosmic ray theory, gamma ray experiments, gamma ray theory

ArXiv ePrint: [2202.03559](https://arxiv.org/abs/2202.03559)

*Corresponding author.



Contents

1	Introduction	1
2	FLUKA cross sections for CR spallation interactions	2
3	Implementation of the FLUKA cross sections in CR propagation codes and compatibility with CR data	6
3.1	Halo size predictions with the FLUKA cross sections	9
3.2	Markov chain Monte Carlo analysis of the diffusion coefficients parameters with the FLUKA cross sections	12
4	Study of the gamma-ray diffuse emission with the FLUKA cross sections	14
5	Conclusions	17
A	Summary of the MCMC results	18
B	^3He FLUKA cross sections	20
C	Electrons and protons spectra	21

1 Introduction

Galactic cosmic rays (CRs) are known to play an important role in the Galaxy, regulating its evolution, shape, mass-metallicity relation, magnetic fields and other processes [1–4]. Understanding their propagation may help reach a better interpretation of the gamma-ray emissions throughout the Milky Way, the characterisation of environmental plasmas or even for indirect searches of dark matter.

The widely accepted standard scenario is that collision-less scatterings of CRs with magneto-hydrodynamic (MHD) plasma waves cause them to follow an erratic motion that can be approximated as a diffusive transport [5–7]. These interactions extend several kiloparsecs above and below the Galactic disk [8–13], constituting the so-called magnetised halo [14]. During their journey, CRs repeatedly cross the Galactic disk undergoing hadronic interactions (spallation reactions) with the gas in the interstellar medium (ISM) and produce secondary particles that can be secondary CRs, gamma rays or neutrinos [15]. These secondary particles are crucial since they bring valuable information on the CR transport and interactions. In particular, the flux ratios of secondary-to-primary CRs (considering as primary CRs those mainly accelerated in astrophysical sources) are commonly used to constrain the propagation parameters defining their transport [16, 17].

Recently, many works have emphasized the need of improving cross sections measurements on spallation reactions in order to reduce the uncertainty related to the determination of the propagation parameters from the secondary-to-primary flux ratios [8, 18–23]. Due to the lack of experimental data in most of the channels and its uncertainty, there have been several attempts to develop the cross-section network purely from physical principles, usually relying on Monte Carlo simulations and event generators. However, as they are mainly adjusted to reproduce accelerator data, they have proved to be less accurate in the region between 100 MeV

to \sim hundreds GeV than the current dedicated parameterisations [22, 24–26]. However, these simulation codes (as, for example, GEANT4 [27], PHITS [28, 29], SHIELD-HIT [30]) have experienced a positive boost in recent years, usually driven by radiological and medical applications, which need to accurately describe the transport of ions in different materials and their interactions.

This paper aims at computing the full cross-section network (including inelastic and inclusive cross sections) needed to be implemented in CR propagation codes, using one of the most recently updated Monte Carlo nuclear codes FLUKA [31–33] and demonstrating its compatibility with data. FLUKA is a general purpose tool that can be used to transport particles in arbitrarily complex geometries, including magnetic fields, through the FLUKA combinatorial geometry. Its application in astroparticle physics studies is one of the main goals of FLUKA, as is demonstrated by a variety of recent works [34–38], raising high expectations in the CR community. This work updates the cross sections calculated by ref. [39], extends its calculations to isotopes up to $Z=26$ and explores in detail the predicted cross sections for B, Be and Li production.

These cross sections are implemented in a private version of the DRAGON2 code¹ [40, 41] in order to demonstrate that they can be used to reproduce the new and accurate CR data with similar accuracy to common analytical and semi-analytical cross sections parameterisations such as the DRAGON2 [8, 42] and GALPROP [43, 44] cross sections, focussing on the study of the secondary CRs B, Be and Li. We employ a Markov chain Monte Carlo (MCMC) analysis, already used in earlier works [45, 46], to determine the propagation parameters from the most recent data from the AMS-02 collaboration [47–57]. A similar analysis was carried out and presented in the third chapter of the author’s PhD thesis [58], where additional details can be found. Furthermore, we derive the cross sections for production of leptons (electrons and positrons) and gamma rays from CR collisions with the interstellar medium and implement them in the `Gammasky` code [59–61] in order to compute gamma-ray sky maps and the local HI emissivity spectrum (see refs. [62, 63] for a discussion on these measurements and predictions). The FLUKA cross sections for secondary lepton production will be discussed in a separate paper (see refs. [64, 65] for recent works on the topic.), more dedicated to the positron spectrum. Also the production of isotopes around the so-called iron group will be discussed in a separate paper.

This paper is organized as follows: in section 2 we discuss the main aspects of the cross-section computations performed and show them in comparison with relevant parameterisations and data. Then, in section 3, we demonstrate that the FLUKA cross sections can be successfully used in a CR propagation code like the DRAGON2 code and report the results of the MCMC analysis for the flux ratios of B, Be and Li over C and O. Section 4 describes the computations of the Galactic diffuse gamma-ray emission with the FLUKA cross sections. Finally, the main highlights are discussed in section 5.

2 FLUKA cross sections for CR spallation interactions

One of the main advantages of using nuclear codes for the computation of cross sections of CR interactions is that it allows us to calculate them for a broad range of energies and species. The possible energy range covered for hadron-hadron and hadron-nucleus interactions in FLUKA extends from a threshold (~ 1 MeV) up to 10^4 TeV, while electromagnetic and muon

¹Available at https://github.com/cosmicrays/DRAGON2-Beta_version.

interactions can be treated from 1 keV (100 eV for photons) up to 10^4 TeV. Nucleus-nucleus interactions are also supported from 1 MeV/n up to 10^4 TeV/n.

FLUKA employs different nuclear models for hadron-nucleus and nucleus-nucleus interactions depending on the energy of the interaction that we are interested in. Below a few GeV, the hadron-nucleon interaction model is based on resonance production and decay of particles, while for higher energies the Dual Parton Model (DPM) is used, implying a treatment in terms of quark chain formation and hadronization. The extension from hadron-nucleon to hadron-nucleus interactions is done in the framework of the PreEquilibrium Approach to NUClear Thermalization model (PEANUT) [66, 67], including the Gribov-Glauber multi-collision mechanism followed by the pre-equilibrium stage and eventually equilibrium processes (evaporation, fission, Fermi break-up and gamma deexcitation). For the nucleus-nucleus interactions, it uses the Boltzmann master equation (BME) [68] below 0.1 GeV/nucleon, while a rQMD (relativistic Quantum Molecular Dynamics) approach [69] is used up to 10 GeV/nucleon. Above this energy, FLUKA is interfaced with DPMJET-III [70]. We refer the reader to ref. [39] and references therein for a more extended description on the interaction models that FLUKA employs for these interactions in different energy ranges. Moreover, full information on the different models used by the code and its related publications and references can be found in the FLUKA webpage.²

Here, we compute the inelastic and inclusive cross sections of all stable isotopes from protons to iron impinging on helium and hydrogen as targets, following the strategy of ref. [39], from 1 MeV/n to 35 TeV/n, using 176 bins equally spaced in a logarithmic scale. Ghost nuclei (i.e. those unstable nuclei, generated via spallation reactions, which have a negligible lifetime compared to typical CR propagation times, and whose contribution is directly added to the cross sections of formation of their daughter nuclei) are carefully taken into account by implementing their decay before calculating the yield of secondary particles produced after the simulated interaction. The results are summarized in a set of spallation and inelastic cross section tables, with the spallation ones calculated for both the direct and cumulative channels, which will be soon publicly available.

Some of the most important inelastic cross sections, for hydrogen as target, computed with FLUKA are shown in figure 1. It shows the proton, helium (as examples of light primary CR), carbon (as an example of heavy primary CR), boron (as an example of secondary CR) and other heavy elements (as a sample of other CR nuclei with very few measurements available) inelastic cross sections calculated with FLUKA and with the CROSEC code³ (also called CRN6) [74] as a function of energy per nucleon, compared to experimental data. For protons, FLUKA adopts the parameterisation found in [75]. Notice that in the case of boron (panel c), the experimental data correspond to the isotopic composition in which it is found in nature ($\sim 80\%$ of ^{11}B and $\sim 20\%$ of ^{10}B , i.e. with average mass number $A \sim 10.8$). Comparisons for the primary CRs ^{20}Ne , ^{24}Mg and ^{28}Si are shown to emphasize the differences found between both computations in channels where the amount of experimental data is very scarce. In fact, as in the case of the spallation inclusive cross sections, parameterisations for inelastic (total) cross sections with few or no experimental data (as in figure 1, f) are just extrapolations of the better measured channels, which may significantly bias the final results. Channels above silicon turn out to be not very important in CR studies of light secondary CRs: they have an impact on the production of light secondary CRs $< 4\%$ for Be and Li, and $< 1\%$ for B (at ~ 10 GeV). In the case of heavier species (figure 1, e, f),

²<http://www.fluka.org/fluka.php?id=publications&mm2=3>.

³This is the default option for inelastic cross sections in the DRAGON2 code.

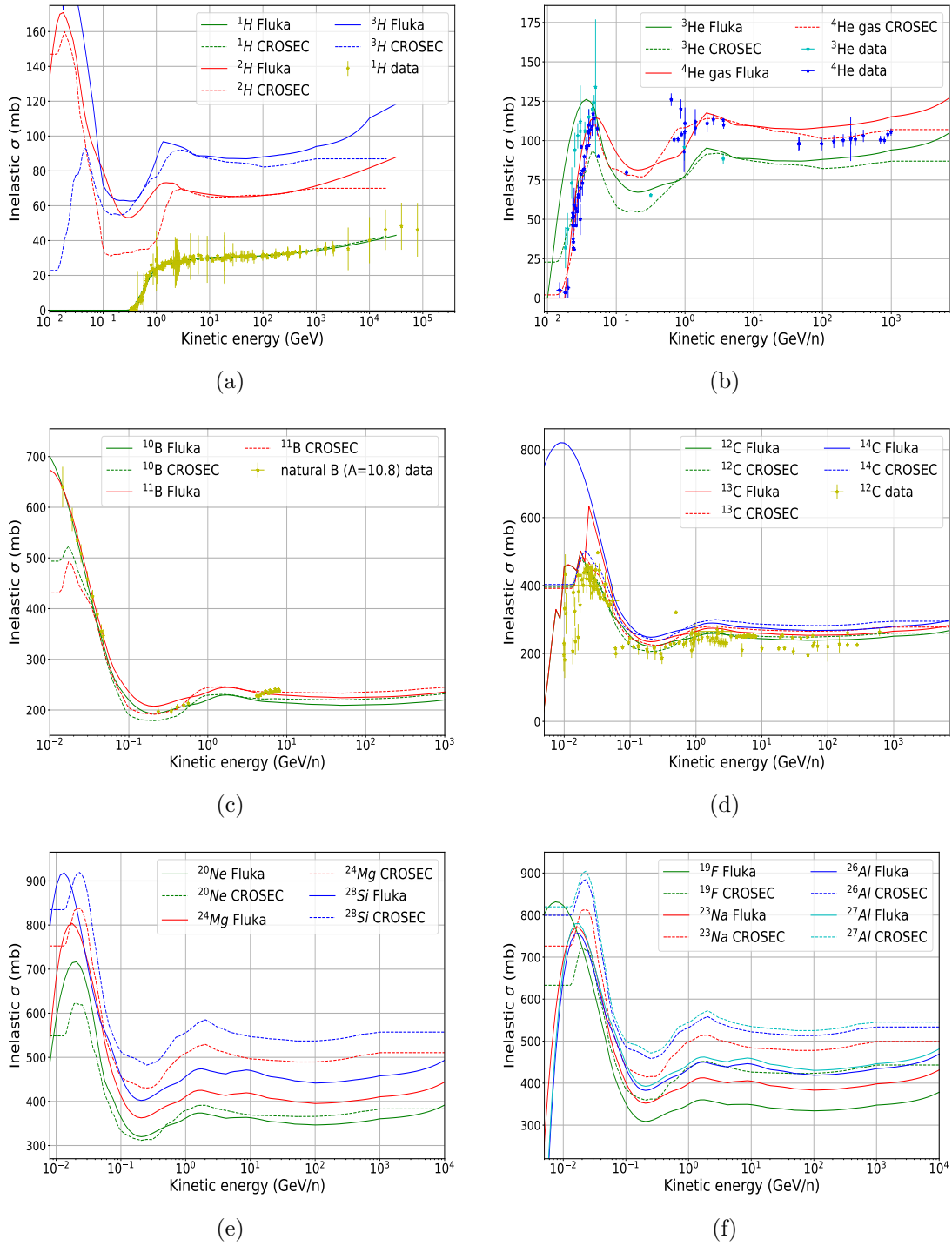


Figure 1. Comparison of the CROSEC and FLUKA inelastic cross sections on hydrogen target for diverse species of projectiles relevant for CR physics: a) protons; b) helium; c) boron; d) carbon; e) other heavier primary CRs (Ne, Mg and Si); f) other heavier secondary CRs (^{19}F , ^{23}Na , ^{26}Al , ^{27}Al). Experimental data are also shown when they are available. Proton-induced reactions data are taken from [71] and are assembled in tables in <http://www.oecd-nea.org/dbdata/bara.html>. Data for heavier nuclei come from a compilation using the EXFOR database [72, 73]. Full references can be found in [22].

discrepancies around 10-20% are found between the two computations at atomic numbers above that of Ne ($Z \geq 10$). For all these heavy nuclei, the energy dependence of their cross sections is very similar. The lack of data in channels involving heavy nuclei makes it specially difficult to adjust a parameterisation (CROSEC) of inelastic cross sections for these nuclei, but, in general, it seems that the inelastic cross sections calculated with FLUKA show a good agreement to the CROSEC parameterisation.

The inclusion of an increase in cross sections at high energies is evident in the FLUKA cross sections, while this is neither incorporated in the inelastic nor in the inclusive cross sections parameterisations, although it has been experimentally observed [76, 77]. This fact can have important implications on the interpretation of the break at high energies in CR spectra, as we comment in appendix A.

The case of inclusive cross sections is more delicate, due to the amount of isotopes involved in the CR network. Figures 2 and 3 show the total (i.e. cross sections of interactions with a gas with ISM composition) cumulative (i.e. including the contribution of ghost nuclei) cross sections of production of the main secondary CR species. The cross sections calculated from FLUKA have a small statistical uncertainty, since it is a Monte Carlo-based computation, that we highlight as a grey band. We compare the computed FLUKA cross sections with the most widely used cross sections parameterisations used in CR codes: the GALPROP and DRAGON2 parameterisations and the cross sections calculated with the WNEW03 [78, 79] and YIELDX [80, 81] (labelled in the legends as TS98) codes. These four cross section models give similar predictions even though they follow different strategies to fit data: whereas the Webber (WNEW03) and DRAGON2 parameterisations followed different phenomenological formulations (and even different experimental data sets to adjust them), the GALPROP cross sections make use of a semi-analytical approach, using Monte Carlo codes in combination with their phenomenological parameterisations and giving special attention to the cross sections measurements more reliable in case there are sizeable discrepancies between experiments in a certain energy region. In contrast, the FLUKA cross sections derived in this work completely relies on theory-based interaction models.

In general, they seem to be consistent with each other, sharing some common trends that should be remarked:

- We find that the FLUKA cumulative cross sections are compatible within 30% with the other cross sections parameterisations. In addition, not only the normalization of these cross sections is compatible with the most updated parameterisations, but their energy dependence seem to be in good agreement.
- The position of the predicted resonances are, in general, in good agreement with those parameterised from data. The main discrepancy is found in the production of ^{10}B , which could also be related to the cross sections from other resonances decaying to ^{10}B , as, e.g., ^{10}C . We highlight here that the different parameterizations also differ in the predicted intensity of resonances, which can be seen from the $^{16}\text{O} \rightarrow ^9\text{Be}$ reaction (upper right panel of figure 3). This would affect our predictions in the energy range of the Voyager-1 data. However, most of the resonances are well reproduced, as can be seen in the $^{12}\text{C} \rightarrow ^{11}\text{B}$ reaction (lower right panel of figure 2).
- One of the main features predicted by the FLUKA cross sections is their smooth rise with energy, which is reliably observed in particle physics experiments [76, 77], but which is not incorporated in any of the current relevant parameterisations. This logarithmic

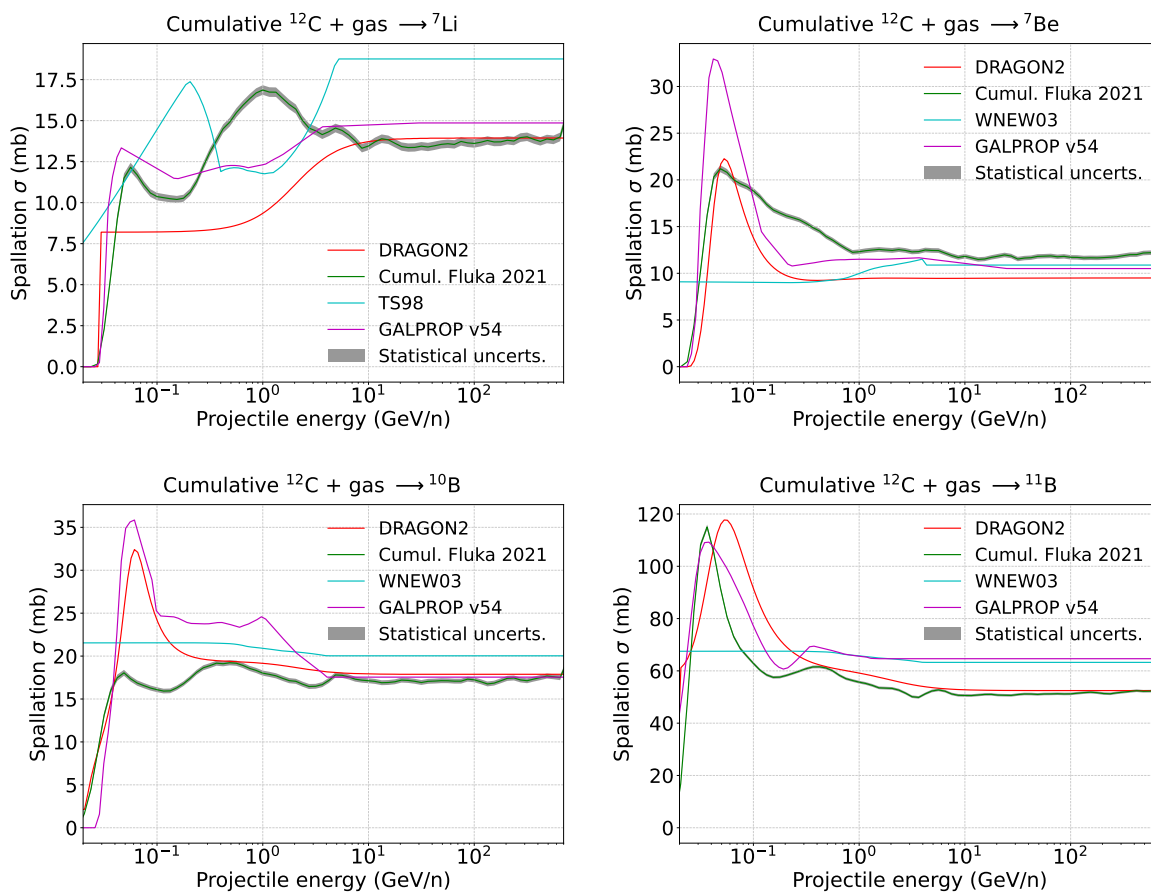


Figure 2. Comparison of the spallation cross sections of CR interactions with ISM gas computed with FLUKA and the most widely used parameterisations, for the production of various isotopes of B, Be and Li from ${}^{12}\text{C}$ as projectile.

rise in the cross sections spectra is present in the FLUKA inelastic and inclusive cross sections, clearer above 100 GeV/n , and can affect our derivations of the spectral index of the diffusion coefficient, δ .

As demonstrated, the FLUKA code is able to make inelastic and spallation cross sections calculations which are, in general, compatible with experimental data and also with the most used and updated parameterisations. Given the scarcity of cross sections measurements (especially for spallation reactions), these nuclear codes, in combination with existent data, are expected to provide a meaningful improvement in the cross sections sets employed for CR studies. In the next section, the capability of the FLUKA cross sections data sets to be consistent with CR data and to provide predictions on CR propagation is studied.

3 Implementation of the FLUKA cross sections in CR propagation codes and compatibility with CR data

The implementation of these new sets of cross sections into the DRAGON2 code has been performed in order to test the reproducibility of the current CR data for all species up to $Z = 26$. The general formula describing the propagation of CRs solved by DRAGON2 is given

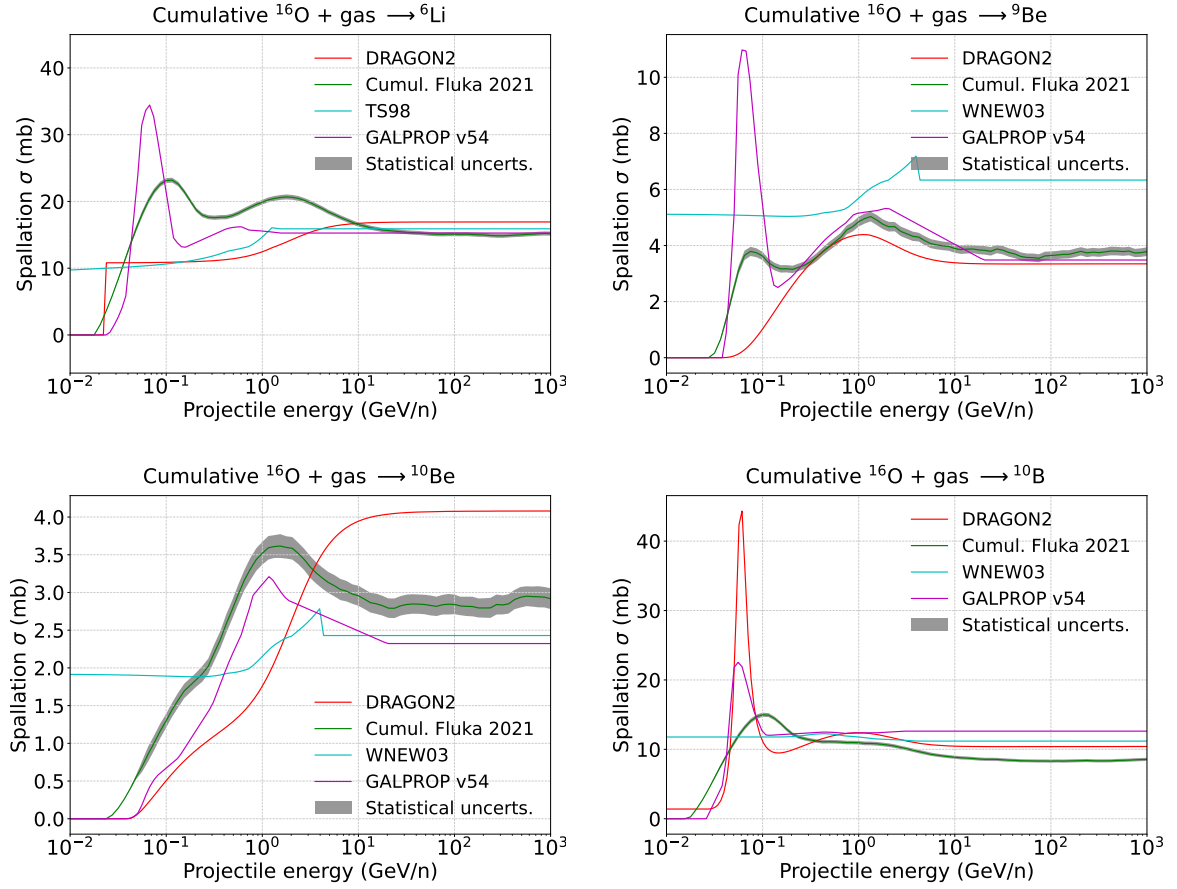


Figure 3. As in figure 2 but for ^{16}O as projectile.

by the following set of equations:

$$\begin{aligned}
 \vec{\nabla} \cdot (\vec{J}_i - \vec{v}_\omega N_i) + \frac{\partial}{\partial p} \left[p^2 D_{pp} \frac{\partial}{\partial p} \left(\frac{N_i}{p^2} \right) \right] &= Q_i + \frac{\partial}{\partial p} \left[\dot{p} N_i - \frac{p}{3} (\vec{\nabla} \cdot \vec{v}_\omega N_i) \right] \\
 - \frac{N_i}{\tau_i^f} + \sum \Gamma_{j \rightarrow i}^s(N_j) - \frac{N_i}{\tau_i^r} + \sum \frac{N_j}{\tau_{j \rightarrow i}^r} & \quad (3.1)
 \end{aligned}$$

Here, \vec{J}_i indicates the CR diffusive flux of the i -th species and N_i is the density per unit momentum. The term \vec{v}_ω represents the advection speed, which we assume to be zero (i.e. we neglect convection). The second term in the left-hand side accounts for the diffusion in momentum space. The first term on the right-hand side, Q_i , represents the distribution and energy spectra of particle sources (injection spectra); the second term describes the momentum losses; finally, the remaining four terms describe losses and gains due to decay and fragmentation.

The same injection and diffusion set-up as presented in refs. [8, 45] is used for the simulations performed with the derived FLUKA cross sections to facilitate comparisons. We have employed two diffusion coefficient parameterisations commonly used in previous works [18, 39, 82], which differ in the interpretation of the high energy break observed in CR data [47, 83–85]. We refer to them as “diffusion” (eq. (3.3)) and “source” (eq. (3.2))

hypotheses, as discussed in ref. [45].

$$D = D_0 \beta^n \left(\frac{R}{R_0} \right)^\delta \quad \text{Source hypothesis} \quad (3.2)$$

$$D = D_0 \beta^n \frac{(R/R_0)^\delta}{\left[1 + (R/R_b)^{\Delta\delta/s} \right]^s} \quad \text{Diffusion hypothesis,} \quad (3.3)$$

where R_0 , the rigidity at which the diffusion coefficient is normalized, is set to 4 GV. For the diffusion coefficient of equation (3.3), we use the values $\Delta\delta = 0.14$, $R_b = 312$ GV and $s = 0.040$, as explained in [45] and derived in ref. [82]. The use of the diffusion coefficient of eq. (3.3) requires using as injection a broken power-law (with break at 8 GV), while the use of that defined in eq. (3.2) requires using a doubly broken power-law (with breaks at 8 GV and 320 GV) for the injection.

We show in figure 4 the spectra of the main primary CRs (mainly dependent on the injection parameters employed) compared to AMS-02. The injection spectra used are freely adjusted to reproduce AMS-02 data. All the experimental data from CR experiments are taken from <https://lpsc.in2p3.fr/crdb/> [86, 87] and <https://tools.ssdc.asi.it/CosmicRays/> [88]. We find here that, in order to reproduce these spectra, we need to employ different injection parameters for ^1H , ^4He , C-O group (i.e. ^{12}C and ^{16}O), Ne-Mg-Si group (^{20}Ne , ^{24}Mg and ^{28}Si), N-Na-Al (^{14}N , ^{23}Na and ^{27}Al) group and Fe (^{56}Fe , ^{57}Fe and ^{58}Fe). These discrepancies may be due to the fact that sources with different properties (as mass or metallicity) may accelerate particles with slightly different power-laws, but the actual reason is still a mystery (see also ref. [89] for a discussion).

Given their importance to study the transport of CRs, we specially focus on the spectra of B, Be and Li and the flux ratios among them, which are depicted in figure 5. These spectra are derived from a Markov chain Monte Carlo analysis (section 3.2) of the AMS-02 boron-over-carbon flux ratio (see figure 7 and upper table 1) for the diffusion coefficient of eq. (3.2). As can be seen from figure 5, there is a $\sim 20 - 25\%$ discrepancy in the Li and Be spectra (right panels of figure 5) with these diffusion parameters, which is well within the uncertainties usually reported in cross sections data [8]. We remark that this discrepancy can be resolved with a $\sim 12\%$ overall increase of the B production cross sections and a $\sim 12\%$ reduction of the Be and Li production cross sections, which predicts the same ratios as for the case with a 25% increase of the B cross sections. Notably, the energy dependence of the derived spectra is well compatible with that of the AMS-02 data for Be, while the Li spectrum seems to be slightly more deviated, as easily seen from their residuals. We notice that the use of the straight-ahead approximation (where the kinetic energy per nucleon of the primary nucleus is conserved in the secondary nucleus) in the DRAGON2 code can affect the predictions of light nuclei at low energy, which would, mainly, add more uncertainty to the low energy part of the Li spectrum. The energy dependence of their respective flux ratios (left column), whose main dependence above 10 GeV/n is the inclusive cross sections, shows this as well. In particular, the predicted Li/Be flux ratio is compatible with AMS-02 data without any scaling of the predicted cross sections above a few GeV/n, while the other ratios need a scaling to be reproduced. In addition, the energy dependence of the predicted Li/B spectrum seems to be slightly discrepant, although still in agreement within the 1σ uncertainties. We have renormalised the B cross sections by 25% to show this more clearly (dashed lines). In appendix B we show the predicted flux of another important light secondary CR, the ^3He isotope, compared to data.

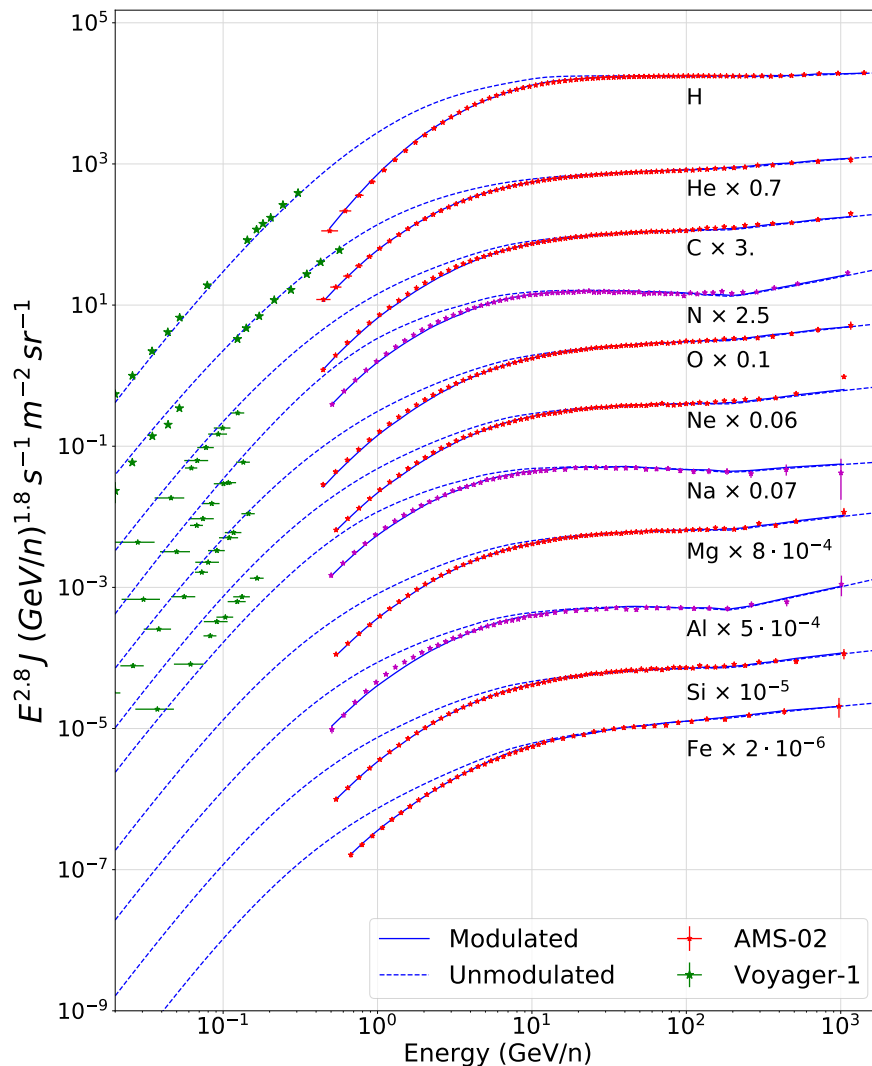


Figure 4. Spectra of the CRs injected in the simulations, compared to AMS-02 and Voyager-1 data (available up to Ne). Modulated spectra (see the text for the details in the Fisk potential used for the data collected in different periods) are shown as a solid line and the unmodulated spectra as a dashed line. Voyager data is shown in green, AMS-02 data corresponding to CR species with a significant secondary contribution (namely N, Na and Al) is shown in magenta and AMS-02 for the main primary CR nuclei is shown in red.

The great importance of having good estimations of the cross sections of production of B, Be and Li derives from the fact that they allow us to constrain the magnetized halo size, the diffusion parameters, the Alfvén velocity and other parameters important for understanding the transport of CRs. These parameters are carefully studied in sections 3.1 and 3.2.

3.1 Halo size predictions with the FLUKA cross sections

The evaluation of the magnetized halo size, i.e. the region in the Galaxy where CRs diffuse, can be constrained from several observables, as radio [13], X-ray and gamma-ray emission [11] from lepton synchrotron and inverse-Compton processes or from other CR observables like unstable heavy nuclei [12], whose mean lifetime is of the order of the propagation time.

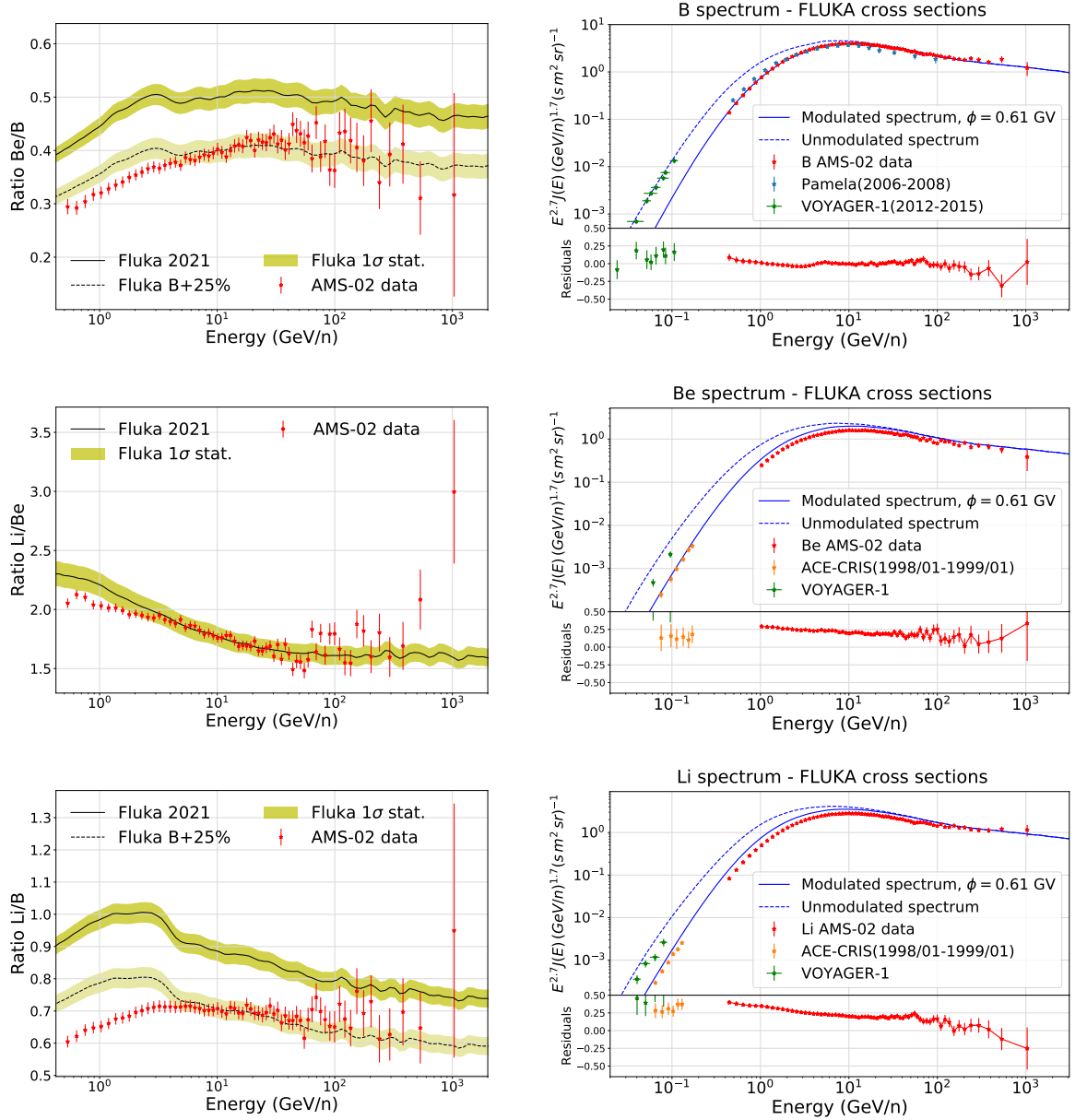


Figure 5. Left column: secondary-over-secondary flux ratios for Li, Be and B obtained with the FLUKA computations, together with the band of statistical uncertainties due to the spallation cross sections calculation (since this is a Monte Carlo computation). Right column: B, Be and Li fluxes obtained from the simulation compared with experimental data, using the diffusion parameters obtained from the fit of the B/C flux ratio (see section 3.2).

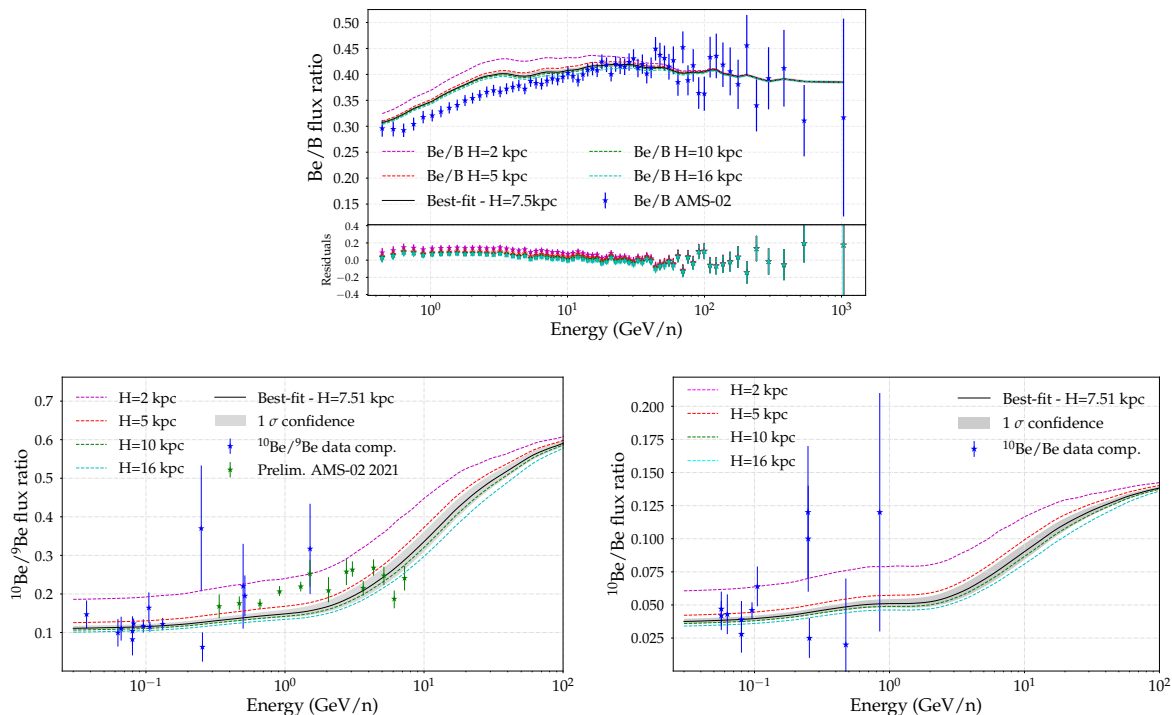


Figure 6. *Top panel:* secondary-over-secondary flux ratios of the light secondary CRs (Li, Be, B). In these plots, the spectrum for the best-fit halo size value found from the $^{10}\text{Be}/^9\text{Be}$ ratios is also shown. *Bottom panels:* $^{10}\text{Be}/^9\text{Be}$ and $^{10}\text{Be}/\text{Be}$ flux ratios. The predictions are compared to experimental data for simulations performed with various halo sizes.

Here, we estimate the magnetized halo size, derived with the FLUKA cross section, from a combined analysis of the ratios of ^{10}Be (mean life time ~ 1.4 My [90]), namely ^{10}Be over ^9Be and ^{10}Be over the total Be flux. To do so, the halo size value is fitted to experimental data on the ^{10}Be flux ratios, from the ACE [91], IMP [92, 93], ISEE [94], ISOMAX [95], Ulysses [96] and Voyager [97] missions, using the `curve_fit` package from the `scipy.optimize` library, as it is done in [8], where we refer the reader for more details about the analysis. This fit yields a value of the halo size of $\sim 7.5_{-0.95}^{+1.13}$ kpc, similar to estimations with other cross sections, usually quoted to be around 6 kpc [8–10] and also favoured by gamma-ray [98] and radio observations [99–101].

In the top panel of figure 6, we display the Be/B flux ratio, with B cross sections scaled by 25%, for various values of the halo size, to show the variations of the predicted ratio for different values of H . In the bottom panel, we show the predicted ^{10}Be ratios for different halo size values. We have also included the $^{10}\text{Be}/^9\text{Be}$ AMS-02 preliminary data in the figure (lower left panel of figure 6) to show that these predictions are compatible with these data as well, but we did not include them in the fit procedure since they are still preliminary. From these figures one can conclude that a halo size value between 5 and 10 kpc would be well compatible with the data. However, we employ the best-fit halo size value in the determination of the other propagation parameters from the secondary-to-primary and secondary-to-primary flux ratios, as explained in the next section.

3.2 Markov chain Monte Carlo analysis of the diffusion coefficients parameters with the FLUKA cross sections

In this section, we show and discuss the results obtained from the analyses carried out for the flux ratios of B, Be and Li to C and O (B/C, B/O, Be/C, Be/O, Li/C and Li/O) and its respective secondary-to-secondary flux ratios (Be/B, Li/B, Li/Be), using the Markov chain Monte Carlo algorithm (MCMC) presented in ref. [45]. We also performed the combined analysis of all these spectra presented in that work, which adds a scale factor to renormalise the cross sections of production of B, Be and Li. The best-fit propagation parameters and their confidence intervals are depicted for both the parameterisations of the diffusion coefficient used, in the form of a box-plot in figure 7 and explicitly given in tables in appendix A. It is convenient to remark on some of the implications of the values found in these analyses of independent ratios:

- An average value of $\delta \sim 0.42$ is favoured by the B and Be ratios, whereas the Li ratios predict a δ value below 0.4. Nevertheless, these values seem to be generally compatible within the 2σ uncertainties in their determination.
- The analyses of the Li and B ratios favour an Alfvén velocity value around 30 km/s, compatible with theoretical estimations [102–104] and with predictions using other cross sections parameterisations [45]. Nevertheless, these values are in tension with energetic considerations, as discussed by ref. [105]. The lower values obtained for V_A in the analyses of the Be ratios were also found for the GALPROP cross sections by ref. [45].
- Notably, η is negative for all the analyses, as revealed by other recent analyses using different cross sections (see, for example, ref. [18]), which reflects a change in the trend of the diffusion coefficient at low energies, towards lower confinement of low-energy CRs. This seems to be due to the dissipation or damping of MHD waves at the scales (Larmor radius of the particles) associated to these energies [106, 107].
- Finally, it can be observed that the D_0/H values obtained are fairly consistent for pairs of ratios with same secondary CR, while the ratios of different secondary CRs significantly deviate, which is due to the spallation cross sections related to the production of each of these secondaries. This highlights the need to add a scale factor for each of these CRs in order to renormalise their cross sections of production.

The combined analyses (i.e. the analyses combining the ratios of the different secondary CRs studied) converge to propagation parameters closer to those predicted by Li ratios. These analyses predict a spectral index of the diffusion coefficient ~ 0.36 , which is significantly lower than the typical values found from B ratios, but which is compatible with the values found for the GALPROP cross sections in ref. [45]. A crucial point of this analysis is the cross sections scale factors obtained. These are the same for both diffusion coefficient parameterisations used and are 1.18, 0.94 and 0.93, for B, Be and Li, respectively, with 1σ statistical uncertainties of $\sim \pm 0.01$. However, we highlight that there are other systematic uncertainties related to the determination of these scale factors, like those related to the inelastic cross sections used, and could make the total systematic uncertainties in the determination of these scale factors to larger than 5% [45]. In addition, we highlight that the diffusion coefficient obtained from these combined analyses allows us to reproduce, at the same time, the ${}^3\text{He}/{}^4\text{He}$ flux ratio (see figure 11), which is evidence that the diffusion coefficient predicted by the light secondary CRs is compatible for the different nuclei within uncertainties (mainly cross sections uncertainties).

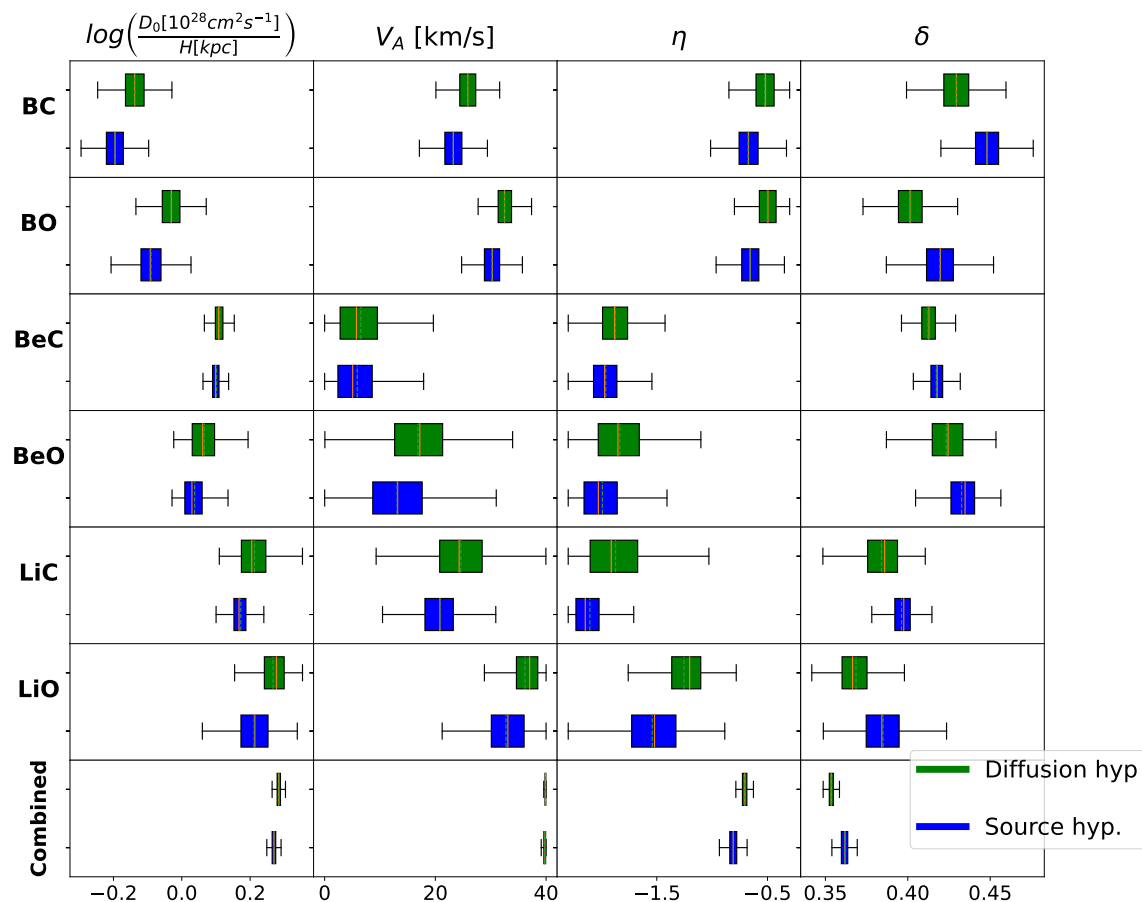


Figure 7. Box-plot summarising the information from the Probability Distribution Function (PDF) of every parameter included in the MCMC analyses performed with the FLUKA cross sections. Different colors represent the different diffusion coefficients employed (eq. (3.2) and eq. (3.3)). This figure is shown in the same format as in ref. [45] to facilitate the comparison with the results obtained from the GALPROP and DRAGON2 cross sections.

The spectra of secondary-to-secondary and secondary-to-primary flux ratios are shown in figure 8 for the best-fit parameters obtained in the combined analysis for the diffusion coefficient of eq. (3.3) (diffusion hypothesis for the origin of the break). These panels demonstrate that the ratios of secondary CRs can be successfully reproduced at the same time with the FLUKA cross sections within 1σ uncertainties, after scaling the overall cross sections of production of B, Be and Li which is well below the typical average uncertainties in the experimental measurements of these cross sections for the best-known channels: $\sim 20\text{--}30\%$, which are those from ^{12}C and ^{16}O as projectiles. We observe small discrepancies at low energies (below 5%) that could be related with these cross sections but could also be related to the parameterisation of the diffusion coefficient used.

It must be highlighted that very few nuclear codes have been able to produce suitable cross sections sets intended to be used in CR propagation codes and none has demonstrated to be able to reproduce the secondary-to-primary flux ratios just with the use of renormalisation (scale) factors. This, in fact, means that the FLUKA cross sections are at the level of precision of the most updated dedicated cross sections parameterisations of CR spallation reactions.

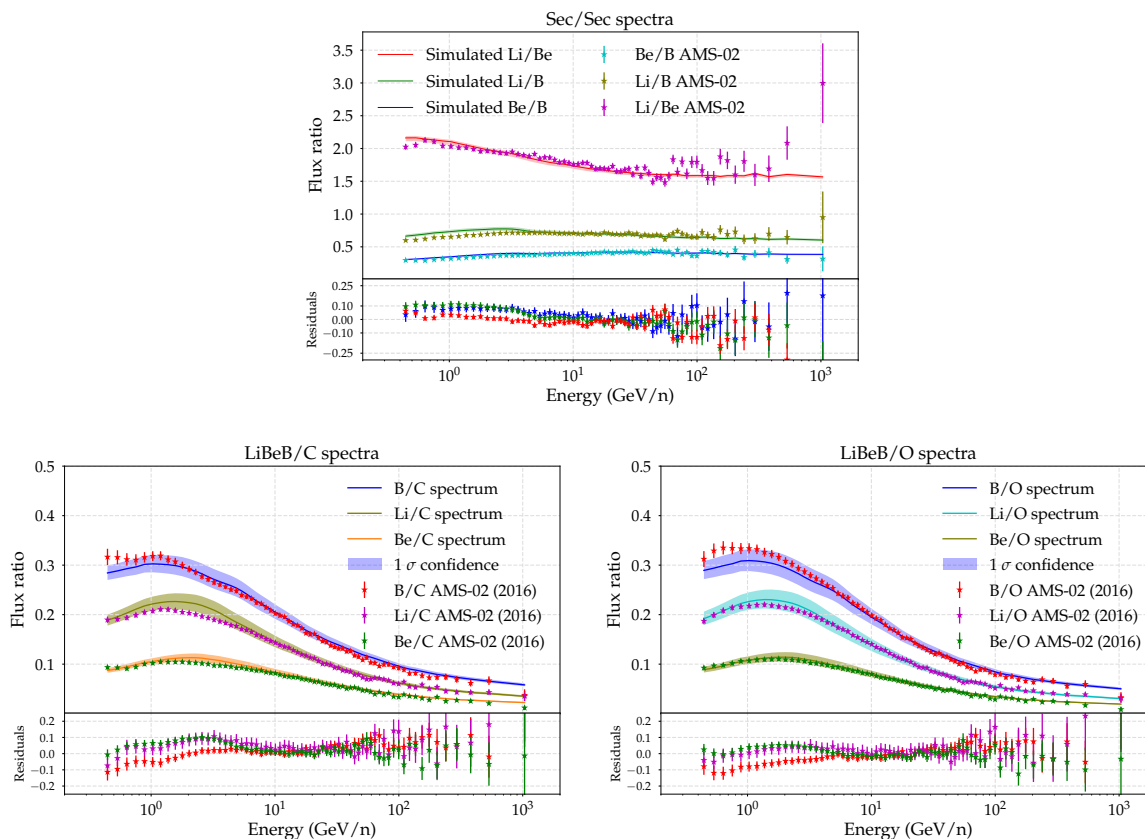


Figure 8. *Top panel:* secondary-over-secondary flux ratios of B, Be and Li computed using the propagation parameters and cross sections scaling factors found in the combined analysis, compared to the AMS-02 experimental data. *Lower panels:* secondary-over-primary spectra (B/C, B/O, Be/C, Be/O, Li/C, Li/O) predicted with the parameters determined by the MCMC combined analysis for the DRAGON2 cross sections. The grid lines at the level of 5% residuals are highlighted in the lower panel in a different color for clarity. In addition, the Voyager-1 data are also included for completeness.

4 Study of the gamma-ray diffuse emission with the FLUKA cross sections

In addition to the information about the transport of CRs from secondary CRs, other secondary particles — namely leptons, antinuclei, gamma rays and neutrinos — are formed and provide essential insight about acceleration mechanisms, magnetic field configurations, environment of sources, etc. An important fraction of the particles produced from spallation reactions of CR nuclei with the ISM gas are short-lived mesons (mainly pions), which are those responsible of the formation of leptons and gamma rays from their decays. Secondary electrons and positrons are mainly produced via the decay of charged pions (accompanied by neutrinos). Gamma rays are mainly produced by the decays of neutral mesons and by the interactions of CR leptons with magnetic and radiation fields in the ISM, carrying important information about the environmental conditions. The study of the Galactic gamma-ray diffuse emission is important to constrain our models and opens a new window to unveil the mechanisms behind CR interactions and acceleration [108, 109].

In this section we demonstrate that the gamma-ray sky maps and the local HI emissivity spectrum, produced using the FLUKA cross sections for the production of leptons and gamma rays from CR interactions with the interstellar gas, are in good agreement with the current

experimental data. We adjust the spectra of protons and leptons with the injection parameters tuned to reproduce AMS-02 data and using the diffusion coefficient given in eq. (3.3), with the parameters obtained in the fit of the B/C spectrum (see figure 12 in appendix C). Here, the CR e^+ and e^- spectra require further considerations: while the vast majority of CR electrons are supposed to be accelerated in supernova remnants (SNRs), a significant amount of positrons seem to be emitted from pulsar wind nebulae (PWN), expected to be symmetric e^+ and e^- pairs emitters [110, 111]. Therefore, to reproduce this component of primary positrons and electrons we inject, in the DRAGON2 simulation, an extra source of leptons (using a single power-law) emitting them in same amount (i.e. no charge asymmetry). We have adjusted this extra component by reproducing the high energy points of the AMS-02 positrons data. In this way, we reproduce the AMS-02 e^+ spectrum as a sum of secondary positrons + primary positrons from extra sources (likely PWN) and the AMS-02 e^- spectrum as primary electrons injected by SNRs + secondary electrons from CR interactions + extra sources (right panel of figure 12). We leave a detailed study of secondary leptons from FLUKA for a separated paper.

Once the CR spectra of these species have been adjusted to match local gamma-ray emissivity values, we compute the gamma-ray diffuse emission by using the `Gammasky` code, a dedicated code able to calculate sky maps of various radiative processes in our Galaxy [39, 59, 112]. Our computation is performed using the gas maps developed by the GALPROP team [108, 113]. The distribution of sources is taken from ref. [114]. Each of its main components and the total gamma-ray intensity predicted at 100 GeV with the FLUKA cross sections are shown in figure 9, together with the Fermi-LAT template of the gamma-ray diffuse emission (lower right panel). Following the calculations performed in ref. [39], the IC, bremsstrahlung and hadronic cross sections of gamma-ray production are calculated with FLUKA assuming an ISM composition with relative abundance of H : He : C : N : O : Ne : Mg : Si = 1 : 0.096 : 4.65×10^{-4} : 8.3×10^{-5} : 8.3×10^{-4} : 1.3×10^{-4} : 3.9×10^{-5} : 3.69×10^{-5} .

As we can see from figure 9, the hadronic emission and bremsstrahlung intensity maps mainly track the gas composition, with the IC component principally probing the ISRF, which is more intense at the Galactic Center. The most recent Fermi-LAT template for the total diffuse emission `gll_iem_v07.fits` (<https://fermi.gsfc.nasa.gov/ssc/data/access/lat/BackgroundModels.html>) is also displayed for comparison. In this template, the contributions from large scale structures, such as the gamma-ray Loop-I [115] and the Fermi Bubbles [116] are also added, which explains the differences observed at high latitudes around the Galactic Center.

Then, in order to avoid the uncertainties related to the gas and radiation fields, we turn our attention to the gamma-ray emissivity produced by the local ISM (LISM). In this context, the local HI emissivity is defined as the diffuse gamma-ray flux, coming from CR interactions with the local gas per unit of gas atom (HI). This quantity is inferred from the Fermi-LAT gamma-ray data [62] and its determination is useful to help constraining different propagation models (see ref. [117] for a derivation of the LISM from this experimental data). The main contribution to the local HI emissivity at low energy originates in Coulomb scattering of CRs with gas and electron bremsstrahlung; a further contribution, dominant above ~ 100 MeV, comes from the gamma-ray emissions of unstable particles formed via nuclear reactions (hadronic emissions). Formally, emissivity can be calculated by means of the following equation:

$$\frac{Q_S(E_S)}{n_{\text{gas}}} = 4\pi \int J(E) \frac{d\sigma(E_S|E)}{dE_S} dE, \quad (4.1)$$

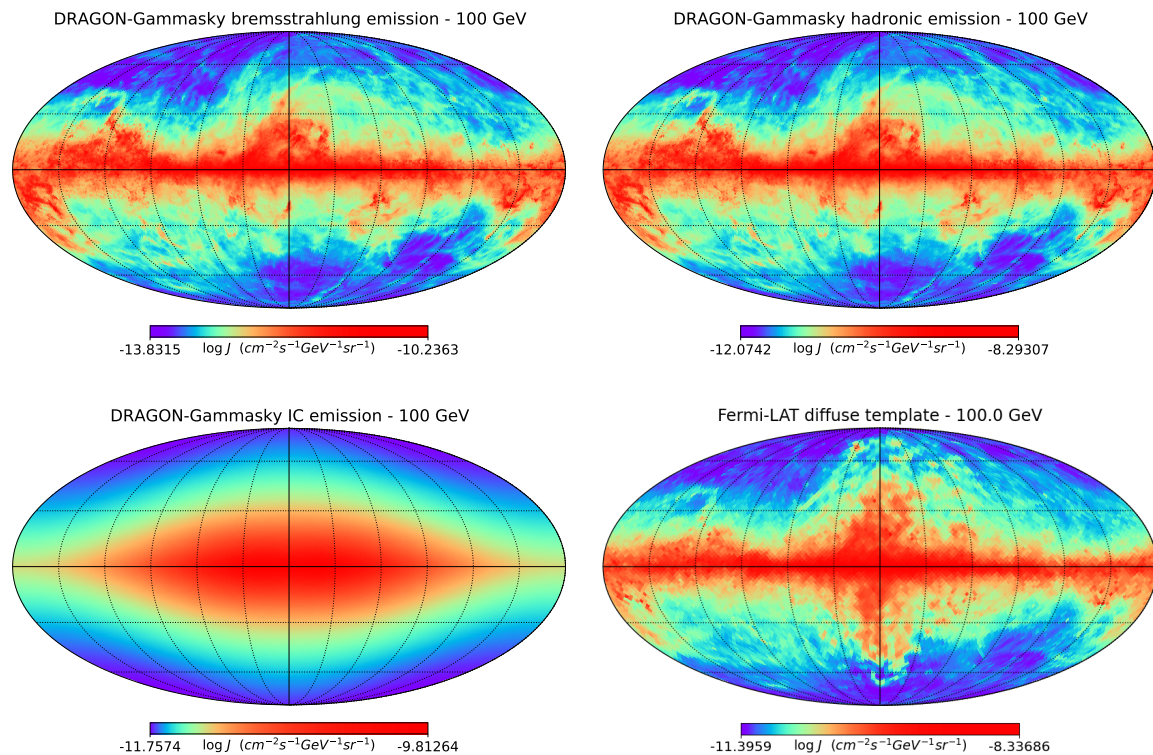


Figure 9. Gamma-ray intensity maps of the Galaxy, in Mollweide projection, for the propagation parameters inferred from the B/C analysis with the FLUKA cross sections. The upper-left map displays the bremsstrahlung emission, the upper-right map the gamma-ray emission from π^0 decays, and the lower-left map the IC emission. The lower-right map is the Fermi-LAT template for the diffuse emission, derived from the 8 first years of operation (PASS 8 data; *P8_R3*, taken from `gll_iem_v07.fits` <https://fermi.gsfc.nasa.gov/ssc/data/access/lat/BackgroundModels.html>).

where n_{gas} is the number of target gas atoms per unit volume and $\sigma(E_S|E)$ the cross section of production of any secondary particle, S, as for example neutrinos, gamma rays, positrons, etc. The ratio $Q_S(E_S)/n_{\text{gas}}$ is expressed in units of $\text{GeV}s^{-1}$.

The computed emissivity spectra, calculated for the propagation parameters derived from the B/C analysis of the FLUKA cross sections, are shown for the diffusion coefficient given in equation (3.3) (diffusion hypothesis) in figure 10. They are compared to the emissivity observed by the Fermi-LAT, inferred from the recent PASS8 data set.⁴

In order to reproduce the local emissivity spectrum at low energies, we are forced to include a low energy break in the injection spectrum of electrons to prevent the bremsstrahlung emission to overpredict the data (or a too small solar modulation potential, which is not in agreement with the rest of observations from neutron monitors and other cosmic rays). This means that we must use a doubly broken power-law injection spectrum for CR electrons, with a low energy break at 8 GeV (note that this is the same break position as for protons), a high energy break at 65 GeV and an exponential cut-off at around 1 TeV (although the AMS-02 spectrum can be perfectly reproduced only with the high energy break and the cut-off). We remark that the high-energy break and cut-off used are in agreement with what other works have recently found [118], however the low energy break is added ad hoc, without a clear theoretical motivation.

⁴These are public data taken from the [Fermi background models website](https://fermi.gsfc.nasa.gov/ssc/data/access/lat/BackgroundModels.html).

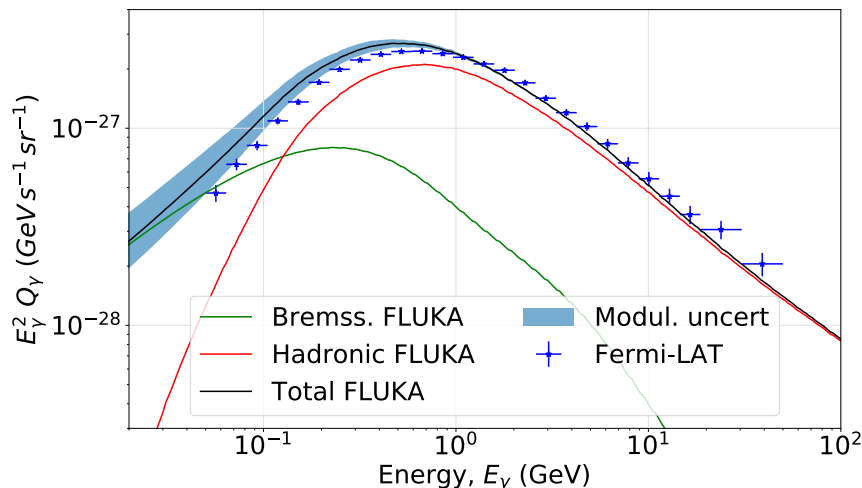


Figure 10. Local HI gamma-ray emissivity spectrum for the propagation parameters derived from the B/C analysis for the FLUKA cross sections. An uncertainty band, for the adjustment of the spectra of p, He and electrons, related to solar modulation uncertainty (variation of ± 0.1 in the Fisk potential) is also shown. Bremsstrahlung and hadronic emissions are also displayed to visualize the region of dominance of each component of the total emissivity. The experimental data is taken from ref. [62].

Finally, it is worth mentioning that, using the FLUKA nuclear code to calculate the gamma-ray production cross sections, we are able to study the gamma-ray emission lines coming from the hadronic interactions of CR protons and helium with ISM nuclei (even being found as traces) such as $p + p \rightarrow \gamma + X$ or $p + {}^{14}\text{N} \rightarrow \gamma + X$. These lines could be detected in the MeV region by the future space experiments like e-Astrogam [119] and have been explored in very few works [120].

5 Conclusions

In this work, the FLUKA calculations for the inelastic and inclusive cross sections important for CR spallation reactions have been presented and their implications discussed. We found that the inelastic cross sections for H, He, B and C are in good agreement with data and are quite similar to the CROSEC predictions at the level of a few percent. Nevertheless, elements with atomic number $Z \geq 10$ (from Ne) start to differ significantly. Then, the total cumulative inclusive cross sections involving the production of Be, Li and B isotopes have been tested in comparison to the most recent dedicated parameterisations, showing a good general agreement, with up to 30% discrepancies.

We evaluate the spectra of secondary CR species after implementing the FLUKA inelastic and inclusive cross sections in the DRAGON2 propagation code, in order to demonstrate that every CR observable can be reproduced with accuracy and at the level of precision of current CR parameterisations. We have studied the B, Be and Li over C and O flux ratios under two different parameterisations of the diffusion coefficient, and the results of these fits and their confidence intervals have been reported. We obtain a best-fit value of the halo size, from the ${}^{10}\text{Be}$ ratios of $H = 7.5_{-0.95}^{+1.13}$ kpc. All these ratios favour a change in the trend of the diffusion coefficient at sub-GeV energies and the predicted slope of the diffusion coefficient, δ , varies from ~ 0.42 (for B and Be ratios) to ~ 0.39 (for Li ratios), which is very similar to what is found from the GALPROP and DRAGON2 parameterisations. We have also performed a

combined analysis of these ratios, which includes also scale factors intended to renormalise the overall FLUKA cross sections of production of B, Be and Li. We have demonstrated that, with the use of these scale factors, we are able to match AMS-02 observations of these secondary-to-primary species within 5% errors above 5 GeV. The scaling factors obtained are of ~ 1.18 , ~ 0.94 and ~ 0.93 for B, Be and Li, respectively, which are below the typical average experimental uncertainties of cross sections measurements for the best known channels (i.e. those from ^{12}C and ^{16}O).

Finally, we have shown the derived diffuse gamma-ray sky maps and the local HI emissivity spectrum using the FLUKA cross sections for production of gamma rays, implemented in the `Gammasky` code. The derived maps are shown to be consistent with the standard picture of the different mechanisms of gamma-ray emission (Inverse-Compton, bremsstrahlung and hadronic decay into photons) in the Galaxy. In addition, we demonstrate that the local HI emissivity spectrum can be well reproduced from the models derived with the FLUKA cross sections, although requiring a low energy break in the injection spectrum of electrons.

In conclusion, the cross sections obtained with the FLUKA code seem to be consistent with the current CR parameterisations and with experimental data, and are able to reproduce every CR observable with a good level of accuracy. They represent a promising tool for future more precise CR studies.

Acknowledgments

P. De la Torre is supported by the Swedish National Space Agency under contract 117/19. We acknowledge the FLUKA collaboration for providing and supporting the code. This work has been partly carried out using the RECAS computing infrastructure in Bari (<https://www.recas-bari.it/index.php/en/>). A particular acknowledgment goes to G. Donvito and A. Italiano for their valuable support. This project used computing resources from the Swedish National Infrastructure for Computing (SNIC) under project Nos. 2021/3-42 and 2021/6-326 partially funded by the Swedish Research Council through grant no. 2018-05973. Some of the discussions included in the text were triggered thanks to the Paris-Saclay Astroparticle Symposium 2021, with the support of the P2IO Laboratory of Excellence (programme ‘‘Investissements d’avenir’’ ANR-11-IDEX-0003-01 Paris-Saclay and ANR-10-LABX-0038), the P2I research departments of the Paris-Saclay university, as well as IJCLab, CEA, IPhT, APPEC, the IN2P3 master projet UCMN and EuCAPT.

A Summary of the MCMC results

In this appendix, the results obtained from the MCMC algorithm of each secondary-to-primary ratio (B/C, B/O, Be/C, Be/O, Li/C, Li/O), in table 1, and their combined analysis, in table 2, for both diffusion parameterisations used (‘Source’ and ‘Diffusion’ hypotheses) are summarized. They contain the median value (coinciding with the maximum posterior probability value) \pm the 1σ uncertainty related to its determination, assuming their PDFs to be Gaussian, and the actual range of values contained in the 95% probability of the distribution.

In table 3, we report tables with the χ^2 values obtained with the best-fit parameters of the independent and combined analyses FLUKA cross sections. Interestingly, we observe that the difference between the χ^2 values from the source and diffusion hypotheses in the independent analyses are of $\Delta\chi^2 \sim 6$, for the B and Li ratios. This yields a significance of $\sim 3.5\sigma$ (making use of Wilk’s theorem), which is 1.2σ less significant than for the DRAGON2

Independent analyses

Source hypothesis						
	B/C	B/O	Be/C	Be/O	Li/C	Li/O
$\frac{D_0 (10^{28} \text{ cm}^2/\text{s})}{H (\text{kpc})}$	0.87 ± 0.03 [0.82, 0.93]	0.97 ± 0.04 [0.89, 1.05]	1.11 ± 0.02 [1.06, 1.16]	1.06 ± 0.05 [0.96, 1.17]	1.22 ± 0.07 [1.1, 1.27]	1.31 ± 0.06 [1.15, 1.41]
v_A (km/s)	25.86 ± 2.16 [21.54, 30.16]	32.4 ± 1.86 [29.01, 35.79]	5.74 ± 5.6 [0., 16.94]	17.02 ± 6.8 [5.52, 29.14]	24.3 ± 6.11 [13.98, 36.52]	37.03 ± 3.73 [29.55, 40.83]
η	-0.53 ± 0.13 [-1.29, -0.8]	-0.51 ± 0.11 [-0.75, -0.31]	-1.88 ± 0.18 [-2.19, -1.52]	-1.85 ± 0.28 [-2.35, -1.29]	-1.91 ± 0.34 [-2.41, -1.29]	-1.23 ± 0.24 [-1.75, -0.92]
δ	0.43 ± 0.01 [0.41, 0.45]	0.40 ± 0.01 [0.38, 0.43]	0.41 ± 0.02 [0.39, 0.44]	0.42 ± 0.01 [0.4, 0.44]	0.39 ± 0.01 [0.37, 0.41]	0.37 ± 0.02 [0.35, 0.4]

Diffusion hypothesis						
	B/C	B/O	Be/C	Be/O	Li/C	Li/O
$\frac{D_0 (10^{28} \text{ cm}^2/\text{s})}{H (\text{kpc})}$	0.82 ± 0.03 [0.88, 0.76]	0.91 ± 0.04 [0.99, 0.83]	1.1 ± 0.02 [1.14, 1.06]	1.03 ± 0.05 [0.94, 1.13]	1.18 ± 0.04 [1.11, 1.26]	1.23 ± 0.07 [1.09, 1.37]
v_A (km/s)	23.26 ± 2.25 [18.6, 27.71]	30.3 ± 2.01 [26.14, 34.16]	5.06 ± 5.2 [0., 15.29]	13.19 ± 6.76 [0., 25.87]	20.82 ± 3.82 [13.18, 28.44]	33.1 ± 4.78 [23.54, 40.64]
η	-0.67 ± 0.13 [-0.93, -0.41]	-0.66 ± 0.11 [-0.88, -0.44]	-1.97 ± 0.17 [-2.26, -1.63]	-2.02 ± 0.26 [-2.4, -1.74]	-2.13 ± 0.19 [-2.37, -1.73]	-1.52 ± 0.32 [-2.16, -1.04]
δ	0.45 ± 0.01 [0.43, 0.47]	0.42 ± 0.01 [0.40, 0.44]	0.42 ± 0.01 [0.40, 0.44]	0.43 ± 0.02 [0.41, 0.45]	0.40 ± 0.02 [0.38, 0.43]	0.38 ± 0.02 [0.37, 0.43]

Table 1. Results obtained in the independent analysis of the flux ratios B/C, Be/C, Li/C, B/O, Be/O and Li/O for the diffusion coefficient parameterisations of eqs. (3.2) and (3.3) for FLUKA the cross sections derived in this work. The halo size value, H , obtained from the ^{10}Be flux ratios was 7.5 kpc.

Combined analysis

Source hypothesis			
$\frac{D_0 (10^{28} \text{ cm}^2/\text{s})}{H (\text{kpc})}$	v_A (km/s)	η	δ
1.33 ± 0.02 [1.29, 1.37]	39.8 ± 0.15 [39.59, 40.02]	-0.72 ± 0.05 [-0.83, -0.62]	0.35 ± 0.02 [0.33, 0.39]

Diffusion hypothesis			
$\frac{D_0 (10^{28} \text{ cm}^2/\text{s})}{H (\text{kpc})}$	v_A (km/s)	η	δ
1.31 ± 0.02 [1.27, 1.35]	39.7 ± 0.33 [39.98, 40.1]	-0.81 ± 0.07 [-0.95, -0.67]	0.36 ± 0.01 [0.34, 0.39]

Table 2. Same as in table 1 but for the combined analysis of the B, Be and Li flux ratios.

χ^2 values of best fit parameters						
	B/C	B/O	Be/C	Be/O	Li/C	Li/O
Source hypothesis Indep. analysis	35.45	27.49	59.01	55.24	57.87	40.45
Diffusion hypothesis Indep. analysis	29.43	22.99	44.47	47.6	51.38	34.13
Source hypothesis Comb. analysis	51.79	32.8	72.33	55.92	63.44	66.56
Diffusion hypothesis Comb. analysis	48.17	32.53	62.77	54.3	60.0	63.52

Table 3. χ^2 values of the best-fit diffusion parameters found for the MCMC analyses with the FLUKA cross sections.

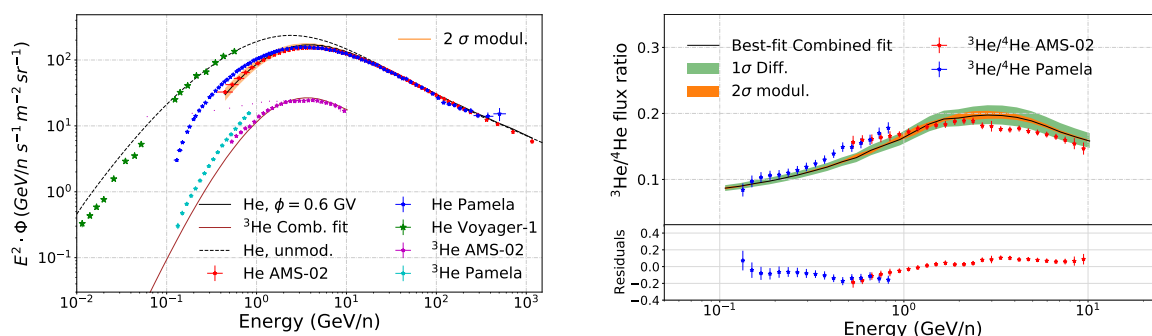


Figure 11. *Left panel:* modulated and unmodulated predicted spectra of He and ^3He compared to AMS-02 and Voyager 1 and Pamela data. *Left panel:* predicted $^3\text{He}/^4\text{He}$ flux ratio compared to Pamela and AMS-02 data. The residuals, calculated as model-data/model are also shown. These spectra are calculated with the diffusion coefficient obtained from the combined fit.

and GALPROP parameterisations, as studied in ref. [45]. This is due to the inclusion of the rise of cross sections at high energies which is not taken into account in the parameterisations and implies that the interpretation of the origin of the break in the CR spectra is sensitive to the cross sections used.

B ^3He FLUKA cross sections

In this appendix we report the predicted flux of another of the main light secondary CRs, the ^3He isotope. We have computed the full ^3He production cross sections from isotopes up to Iron ($Z = 26$). The contribution to the total ^3He flux from nuclei heavier than He is, in average, $\sim 44\%$. As we observe from figure 11, the predicted ^3He flux, with the diffusion coefficient obtained in the combined analysis, is reasonably compatible with data in both, energy-dependence and intensity. We also include data from the PAMELA mission [83] in this figure, taken in the period from 2006/07 to 2008/12. It is worth mentioning that the predicted ^3He flux with the diffusion coefficient obtained in the independent B/C analysis is overpredicted in the energy region between 1 GeV and 10 GeV by around 20%.

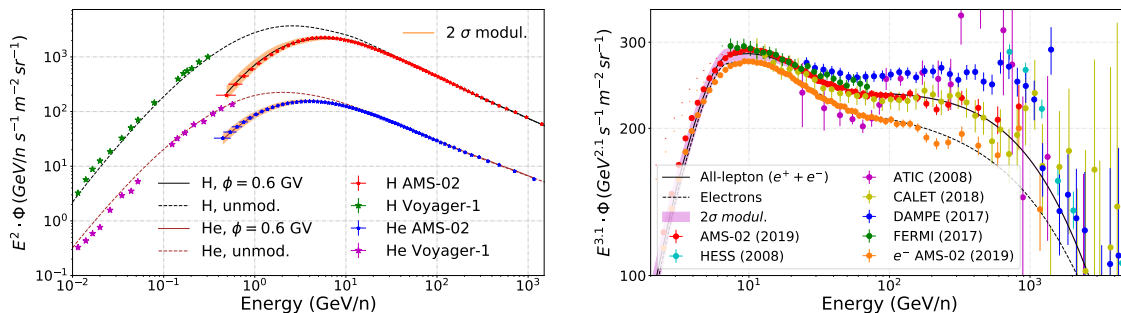


Figure 12. *Left panel:* modulated and unmodulated predicted spectra of H and He compared to AMS-02 and Voyager 1 data. *Right panel:* predicted total CRE spectra compared to AMS-02, Fermi-LAT, DAMPE and CALET data. The dashed line represents the predicted flux of electrons, fitting to the AMS-02 electron flux. The uncertainty band related to a variation of the Fisk potential of ± 0.1 GV is shown for the spectra in both figures.

C Electrons and protons spectra

In this appendix we show the evaluated spectra of proton, helium and leptons. These are obtained by tuning the injection spectra to reproduce experimental data. In the case of protons and helium, we also include the Voyager-01 data. The reproduction of the CR electrons spectrum (CRE) involves also choosing a configuration of the magnetic field and the radiation fields. The DRAGON2 code allows the parameterisation of three components of the magnetic field (see ref. [121]): one for the disc, one for the halo and a turbulent one. We set the magnetic field parameters to $B_{\text{disc}} = 2\mu\text{G}$, $B_{\text{halo}} = 4\mu\text{G}$ and $B_{\text{turb}} = 7.5\mu\text{G}$ as found in ref. [118]. The energy density of the radiation fields, important for the energy losses related to IC scattering, were taken from ref. [122].

The computed proton and helium spectra are shown in figure 12, left, compared to Voyager-1 [123] (unmodulated) and AMS-02 [48] (using a Fisk potential $\phi = 0.6$ GV). The electron and total CRE spectra are compared to data, from Fermi-LAT [124], DAMPE [125], CALET [126] and AMS-02 [127], in the right panel of figure 12. These spectra are derived using the propagation parameters inferred from the B/C analysis with the FLUKA cross sections in the diffusion approximation. The uncertainty band related to a variation of the Fisk potential of ± 0.1 GV is included for these spectra.

References

- [1] R.S. Somerville and R. Davé, *Physical Models of Galaxy Formation in a Cosmological Framework*, *Ann. Rev. Astron. Astrophys.* **53** (2015) 51 [[arXiv:1412.2712](#)] [[INSPIRE](#)].
- [2] P.F. Hopkins et al., *But what about...: cosmic rays, magnetic fields, conduction, and viscosity in galaxy formation*, *Mon. Not. Roy. Astron. Soc.* **492** (2020) 3465 [[arXiv:1905.04321](#)] [[INSPIRE](#)].
- [3] I.A. Grenier, J.H. Black and A.W. Strong, *The Nine Lives of Cosmic Rays in Galaxies*, *Ann. Rev. Astron. Astrophys.* **53** (2015) 199 [[INSPIRE](#)].
- [4] R. Farber, M. Ruszkowski, H.Y.K. Yang and E.G. Zweibel, *Impact of Cosmic Ray Transport on Galactic Winds*, *Astrophys. J.* **856** (2018) 112 [[arXiv:1707.04579](#)] [[INSPIRE](#)].
- [5] S. Gabici et al., *The origin of Galactic cosmic rays: challenges to the standard paradigm*, *Int. J. Mod. Phys. D* **28** (2019) 1930022 [[arXiv:1903.11584](#)] [[INSPIRE](#)].

- [6] V.L. Ginzburg and S.I. Syrovatskii, *The origin of cosmic rays*, Gordon & Breach Publishing Group, London, U.K. (1969).
- [7] V. Berezhinskii, V. Dogiel, S. Bulanov and V.L. Ginzburg, *Astrophysics of cosmic rays*, vol. 393, North-Holland, Amsterdam, The Netherlands (1990).
- [8] P. De La Torre Luque, M.N. Mazziotta, F. Loparco, F. Gargano and D. Serini, *Implications of current nuclear cross sections on secondary cosmic rays with the upcoming DRAGON2 code*, *JCAP* **03** (2021) 099 [[arXiv:2101.01547](#)] [[INSPIRE](#)].
- [9] C. Evoli, G. Morlino, P. Blasi and R. Aloisio, *AMS-02 beryllium data and its implication for cosmic ray transport*, *Phys. Rev. D* **101** (2020) 023013 [[arXiv:1910.04113](#)] [[INSPIRE](#)].
- [10] N. Weinrich et al., *Galactic halo size in the light of recent AMS-02 data*, *Astron. Astrophys.* **639** (2020) A74 [[arXiv:2004.00441](#)] [[INSPIRE](#)].
- [11] S. Biswas and N. Gupta, *Constraining the halo size from possible density profiles of hydrogen gas of Milky Way Galaxy*, *JCAP* **07** (2018) 063 [[arXiv:1802.03538](#)] [[INSPIRE](#)].
- [12] I.V. Moskalenko and A.W. Strong, *Diffuse galactic gamma-rays: constraining cosmic-ray origin and propagation*, *Astrophys. Space Sci.* **272** (2000) 247 [[astro-ph/9908032](#)] [[INSPIRE](#)].
- [13] T. Bringmann, F. Donato and R.A. Lineros, *Radio data and synchrotron emission in consistent cosmic ray models*, *JCAP* **01** (2012) 049 [[arXiv:1106.4821](#)] [[INSPIRE](#)].
- [14] S. Stephens and R. Streitmatter, *Cosmic-ray propagation in the galaxy: Techniques and the mean matter traversal*, *Astrophys. J.* **505** (1998) 266.
- [15] J. Becker Tjus and L. Merten, *Closing in on the origin of Galactic cosmic rays using multimessenger information*, *Phys. Rept.* **872** (2020) 1 [[arXiv:2002.00964](#)] [[INSPIRE](#)].
- [16] A. Reinert and M.W. Winkler, *A Precision Search for WIMPs with Charged Cosmic Rays*, *JCAP* **01** (2018) 055 [[arXiv:1712.00002](#)] [[INSPIRE](#)].
- [17] L. Derome, D. Maurin, P. Salati, M. Boudaud, Y. Génolini and P. Kunzé, *Fitting B/C cosmic-ray data in the AMS-02 era*, *PoS ICRC2019* (2020) 054 [[INSPIRE](#)].
- [18] N. Weinrich, Y. Génolini, M. Boudaud, L. Derome and D. Maurin, *Combined analysis of AMS-02 (Li, Be, B)/C, N/O, ^3He , and ^4He data*, *Astron. Astrophys.* **639** (2020) A131 [[arXiv:2002.11406](#)] [[INSPIRE](#)].
- [19] M. Korsmeier and A. Cuoco, *Implications of Lithium to Oxygen AMS-02 spectra on our understanding of cosmic-ray diffusion*, *Phys. Rev. D* **103** (2021) 103016 [[arXiv:2103.09824](#)] [[INSPIRE](#)].
- [20] P. De la Torre Luque, F. Gargano, F. Loparco, M.N. Mazziotta and D. Serini, *New Markov-Chain Monte Carlo analyses for the evaluation of the antiproton background*, *J. Phys. Conf. Ser.* **1690** (2020) 012010 [[INSPIRE](#)].
- [21] P. Gondolo, *Wanted! Nuclear Data for Dark Matter Astrophysics*, *Nucl. Data Sheets* **120** (2014) 175 [[arXiv:1311.6038](#)] [[INSPIRE](#)].
- [22] Y. Génolini, D. Maurin, I.V. Moskalenko and M. Unger, *Current status and desired precision of the isotopic production cross sections relevant to astrophysics of cosmic rays: Li, Be, B, C, and N*, *Phys. Rev. C* **98** (2018) 034611 [[arXiv:1803.04686](#)] [[INSPIRE](#)].
- [23] N. Tomassetti, *Examination of uncertainties in nuclear data for cosmic ray physics with the AMS experiment*, *Phys. Rev. C* **92** (2015) 045808 [[arXiv:1509.05776](#)] [[INSPIRE](#)].
- [24] S.G. Mashnik, *Validation and Verification of MCNP6 Against Intermediate and High-Energy Experimental Data and Results by Other Codes*, *Eur. Phys. J. Plus* **126** (2011) 49 [[arXiv:1011.4978](#)] [[INSPIRE](#)].

- [25] S.G. Mashnik, L.M. Kerby, K.K. Gudima, A.J. Sierk, J.S. Bull and M.R. James, *Production of energetic light fragments in extensions of the CEM and LAQGSM event generators of the Monte Carlo transport code MCNP6*, *Phys. Rev. C* **95** (2017) 034613 [[arXiv:1607.02506](#)] [[INSPIRE](#)].
- [26] L.M. Kerby and S.G. Mashnik, *Total Reaction Cross Sections in CEM and MCNP6 at Intermediate Energies*, *Nucl. Instrum. Meth. B* **356-357** (2015) 135 [[arXiv:1505.00842](#)] [[INSPIRE](#)].
- [27] I. Pshenichnov, A. Botvina, I. Mishustin and W. Greiner, *Nuclear fragmentation reactions in extended media studied with geant4 toolkit*, *Nucl. Instrum. Meth. B* **268** (2010) 604.
- [28] K. Niita et al., *Analysis of the (N, xN') reactions by quantum molecular dynamics plus statistical decay model*, *Phys. Rev. C* **52** (1995) 2620 [[nucl-th/9508004](#)] [[INSPIRE](#)].
- [29] L. Sihver et al., *An update about recent developments of the phits code*, *Adv. Space Res.* **45** (2010) 892.
- [30] M. Hultqvist, M. Lazzeroni, A. Botvina, I. Gudowska, N. Sobolevsky and A. Brahme, *Evaluation of nuclear reaction cross-sections and fragment yields in carbon beams using the SHIELD-HIT Monte Carlo code. Comparison with experiments*, *Phys. Med. Biol.* **57** (2012) 4369.
- [31] A. Ferrari, P.R. Sala, A. Fasso and J. Ranft, *FLUKA: A multi-particle transport code (Program version 2005)*, [[INSPIRE](#)].
- [32] A. Fasso, A. Ferrari, J. Ranft and P.R. Sala, *FLUKA: Present status and future developments*, *Conf. Proc. C* **9309194** (1993) 493 [[INSPIRE](#)].
- [33] G. Aricò et al., *Developments of the nuclear reaction and fragmentation models in FLUKA for ion collisions at therapeutic energies*, *CERN Proc.* **1** (2019) 321 [[INSPIRE](#)].
- [34] FLUKA collaboration, *The FLUKA code, galactic cosmic ray and Solar Energetic Particle events: From fundamental physics to space radiation and commercial aircraft doses*, in *2008 IEEE Nuclear Science Symposium and Medical Imaging Conference*, pp. 1609–1615 (2008) [[DOI](#)].
- [35] V. Andersen et al., *The fluka code for space applications: recent developments*, *Adv. Space Res.* **34** (2004) 1302 [[INSPIRE](#)].
- [36] J.H. Heinbockel et al., *Comparison of the transport codes HZETRN, HETC and FLUKA for galactic cosmic rays*, *Adv. Space Res.* **47** (2011) 1089 [[INSPIRE](#)].
- [37] D.S. Tusnski, S. Szpigiel, C.G. Giménez de Castro, A.L. MacKinnon and P.J.A. Simões, *Self-consistent Modeling of Gamma-ray Spectra from Solar Flares with the Monte Carlo Simulation Package FLUKA*, *Solar Phys.* **294** (2019) 103 [[arXiv:1907.11575](#)] [[INSPIRE](#)].
- [38] M.N. Mazziotta et al., *Cosmic-ray interactions with the Sun using the FLUKA code*, *Phys. Rev. D* **101** (2020) 083011 [[arXiv:2001.09933](#)] [[INSPIRE](#)].
- [39] M.N. Mazziotta, F. Cerutti, A. Ferrari, D. Gaggero, F. Loparco and P.R. Sala, *Production of secondary particles and nuclei in cosmic rays collisions with the interstellar gas using the FLUKA code*, *Astropart. Phys.* **81** (2016) 21 [[arXiv:1510.04623](#)] [[INSPIRE](#)].
- [40] C. Evoli et al., *Cosmic-ray propagation with DRAGON2: I. numerical solver and astrophysical ingredients*, *JCAP* **02** (2017) 015 [[arXiv:1607.07886](#)] [[INSPIRE](#)].
- [41] C. Evoli, D. Gaggero, A. Vittino, M. Di Mauro, D. Grasso and M.N. Mazziotta, *Cosmic-ray propagation with DRAGON2: II. Nuclear interactions with the interstellar gas*, *JCAP* **07** (2018) 006 [[arXiv:1711.09616](#)] [[INSPIRE](#)].
- [42] C. Evoli, R. Aloisio and P. Blasi, *Galactic cosmic rays after the AMS-02 observations*, *Phys. Rev. D* **99** (2019) 103023 [[arXiv:1904.10220](#)] [[INSPIRE](#)].

- [43] I.V. Moskalenko and S.G. Mashnik, *Evaluation of production cross sections of Li, Be, B in CR, in 28th International Cosmic Ray Conference*, pp. 1969–1972 (2003) [[astro-ph/0306367](#)] [[INSPIRE](#)].
- [44] I.V. Moskalenko, A.W. Strong and S.G. Mashnik, *Propagation of cosmic rays: Nuclear physics in cosmic-ray studies*, *AIP Conf. Proc.* **769** (2005) 1612 [[astro-ph/0411400](#)] [[INSPIRE](#)].
- [45] P.D.L.T. Luque, M.N. Mazziotta, F. Loparco, F. Gargano and D. Serini, *Markov chain Monte Carlo analyses of the flux ratios of B, Be and Li with the DRAGON2 code*, *JCAP* **07** (2021) 010 [[arXiv:2102.13238](#)] [[INSPIRE](#)].
- [46] P.D.L.T. Luque, *Combined analyses of the antiproton production from cosmic-ray interactions and its possible dark matter origin*, *JCAP* **11** (2021) 018 [[arXiv:2107.06863](#)] [[INSPIRE](#)].
- [47] AMS collaboration, *First Result from the Alpha Magnetic Spectrometer on the International Space Station: Precision Measurement of the Positron Fraction in Primary Cosmic Rays of 0.5–350 GeV*, *Phys. Rev. Lett.* **110** (2013) 141102 [[INSPIRE](#)].
- [48] AMS collaboration, *Precision Measurement of the Proton Flux in Primary Cosmic Rays from Rigidity 1 GV to 1.8 TV with the Alpha Magnetic Spectrometer on the International Space Station*, *Phys. Rev. Lett.* **114** (2015) 171103 [[INSPIRE](#)].
- [49] AMS collaboration, *Precision Measurement of Cosmic-Ray Nitrogen and its Primary and Secondary Components with the Alpha Magnetic Spectrometer on the International Space Station*, *Phys. Rev. Lett.* **121** (2018) 051103 [[INSPIRE](#)].
- [50] AMS collaboration, *Properties of Neon, Magnesium, and Silicon Primary Cosmic Rays Results from the Alpha Magnetic Spectrometer*, *Phys. Rev. Lett.* **124** (2020) 211102 [[INSPIRE](#)].
- [51] AMS collaboration, *Observation of the Identical Rigidity Dependence of He, C, and O Cosmic Rays at High Rigidities by the Alpha Magnetic Spectrometer on the International Space Station*, *Phys. Rev. Lett.* **119** (2017) 251101 [[INSPIRE](#)].
- [52] AMS collaboration, *Observation of New Properties of Secondary Cosmic Rays Lithium, Beryllium, and Boron by the Alpha Magnetic Spectrometer on the International Space Station*, *Phys. Rev. Lett.* **120** (2018) 021101 [[INSPIRE](#)].
- [53] AMS collaboration, *Towards Understanding the Origin of Cosmic-Ray Electrons*, *Phys. Rev. Lett.* **122** (2019) 101101 [[INSPIRE](#)].
- [54] AMS COLLABORATION collaboration, *Properties of a new group of cosmic nuclei: Results from the alpha magnetic spectrometer on sodium, aluminum, and nitrogen*, *Phys. Rev. Lett.* **127** (2021) 021101.
- [55] AMS collaboration, *Properties of Iron Primary Cosmic Rays: Results from the Alpha Magnetic Spectrometer*, *Phys. Rev. Lett.* **126** (2021) 041104 [[INSPIRE](#)].
- [56] AMS collaboration, *Towards Understanding the Origin of Cosmic-Ray Positrons*, *Phys. Rev. Lett.* **122** (2019) 041102 [[INSPIRE](#)].
- [57] AMS collaboration, *Properties of Heavy Secondary Fluorine Cosmic Rays: Results from the Alpha Magnetic Spectrometer*, *Phys. Rev. Lett.* **126** (2021) 081102 [[INSPIRE](#)].
- [58] P.d.l.T. Luque, *Cosmic-ray propagation and production of secondary particles in the Galaxy*, Ph.D. Thesis, Università degli Studi di Bari, Bari, Italy (2020) [[arXiv:2202.07063](#)] [[INSPIRE](#)].
- [59] M. Cirelli, D. Gaggero, G. Giesen, M. Taoso and A. Urbano, *Antiproton constraints on the GeV gamma-ray excess: a comprehensive analysis*, *JCAP* **12** (2014) 045 [[arXiv:1407.2173](#)] [[INSPIRE](#)].
- [60] C. Evoli, D. Gaggero, D. Grasso and L. Maccione, *A common solution to the cosmic ray anisotropy and gradient problems*, *Phys. Rev. Lett.* **108** (2012) 211102 [[arXiv:1203.0570](#)] [[INSPIRE](#)].

- [61] M. Tavakoli, I. Cholis, C. Evoli and P. Ullio, *Diffuse Galactic Gamma Rays at Intermediate and High Latitudes, Constraints on ISM Properties*, in *3rd International Fermi Symposium*, (2011) [[arXiv:1110.5922](#)] [[INSPIRE](#)].
- [62] J.-M. Casandjian, *Local HI emissivity measured with Fermi-LAT and implications for cosmic-ray spectra*, *Astrophys. J.* **806** (2015) 240 [[arXiv:1506.00047](#)] [[INSPIRE](#)].
- [63] E. Orlando, *Imprints of Cosmic Rays in Multifrequency Observations of the Interstellar Emission*, *Mon. Not. Roy. Astron. Soc.* **475** (2018) 2724 [[arXiv:1712.07127](#)] [[INSPIRE](#)].
- [64] L. Orusa, M. Di Mauro, F. Donato and M. Korsmeier, *New determination of the production cross section for secondary positrons and electrons in the Galaxy*, *Phys. Rev. D* **105** (2022) 123021 [[arXiv:2203.13143](#)] [[INSPIRE](#)].
- [65] S. Koldobskiy, M. Kachelrieß, A. Lskavyan, A. Neronov, S. Ostapchenko and D.V. Semikoz, *Energy spectra of secondaries in proton-proton interactions*, *Phys. Rev. D* **104** (2021) 123027 [[arXiv:2110.00496](#)] [[INSPIRE](#)].
- [66] A. Fassò, A. Ferrari, P.R. Sala and J. Ranft, *FLUKA: Status and prospects for hadronic applications*, in *Advanced Monte Carlo for radiation physics, particle transport simulation and applications*, MC2000, Lisbon, Portugal, 23–26 October 2000, pp. 955–960 (2000) [[INSPIRE](#)].
- [67] G. Battistoni et al., *Recent developments in the FLUKA nuclear reaction models*, in *Proc. 11th Int. Conf. Nucl. React. Mech.*, Università degli studi di Milano, Milano, Italy, pp. 483–95 (2006).
- [68] V.A. Guseinov, R.E. Gasimova and I.G. Jafarov, *Antineutrino-electron scattering in a magnetic field with allowance for polarizations of electrons*, *J. Phys. G* **34** (2007) 897 [[INSPIRE](#)].
- [69] A. Rose, *A systematic comparison of RQMD to $p + A$ data*, in *Centennial Celebration and Meeting of the American Physical Society*, pp. 36–40 (1999) [[INSPIRE](#)].
- [70] S. Roesler, R. Engel and J. Ranft, *The Monte Carlo event generator DPMJET-III*, *Proceedings of the Monte Carlo 2000 Conference*, (2001) [[DOI](#)].
- [71] B.M. Bobchenko et al., *Measurement of total inelastic cross-sections from proton interactions with nuclei in the momentum range from 5-GeV/c to 9-GeV/c and pi-mesons with nuclei in the momentum range from 1.75-GeV/c to 6.5-GeV/c*, *Sov. J. Nucl. Phys.* **30** (1979) 805 [[INSPIRE](#)].
- [72] N. Otuka et al., *Towards a More Complete and Accurate Experimental Nuclear Reaction Data Library (EXFOR): International Collaboration Between Nuclear Reaction Data Centres (NRDC)*, *Nucl. Data Sheets* **120** (2014) 272 [[arXiv:2002.07114](#)] [[INSPIRE](#)].
- [73] V. Zerkin and B. Pritychenko, *The experimental nuclear reaction data (EXFOR): Extended computer database and web retrieval system*, *Nucl. Instrum. Meth. A* **888** (2018) 31.
- [74] V.S. Barashenkov and A. Polanski, *Electronic guide for nuclear cross-sections: version 1994*, [E2-94-417](#), JINR-E2-94-417 (1994).
- [75] E. Kafexhiu, F. Aharonian, A.M. Taylor and G.S. Vila, *Parametrization of gamma-ray production cross-sections for pp interactions in a broad proton energy range from the kinematic threshold to PeV energies*, *Phys. Rev. D* **90** (2014) 123014 [[arXiv:1406.7369](#)] [[INSPIRE](#)].
- [76] M.M. Block, L. Durand, P. Ha and F. Halzen, *Comprehensive fits to high energy data for σ , ρ , and B and the asymptotic black-disk limit*, *Phys. Rev. D* **92** (2015) 114021 [[arXiv:1511.02406](#)] [[INSPIRE](#)].
- [77] M.M. Block and F. Halzen, *Experimental Confirmation that the Proton is Asymptotically a Black Disk*, *Phys. Rev. Lett.* **107** (2011) 212002 [[arXiv:1109.2041](#)] [[INSPIRE](#)].
- [78] W. Webber, A. Soutoul, J. Kish and J. Rockstroh, *Updated formula for calculating partial cross sections for nuclear reactions of nuclei with $z \leq 28$ and $E > 150$ MeV nucleon⁻¹ in hydrogen targets*, *Astrophys. J. Suppl. Ser.* **144** (2003) 153.

- [79] W.R. Webber, J.C. Kish and D.A. Schrier, *Formula for calculating partial cross-sections for nuclear reactions of nuclei with $E \gtrsim 200$ MeV/nucleon in hydrogen targets*, *Phys. Rev. C* **41** (1990) 566 [INSPIRE].
- [80] C. Tsao, R. Silberberg and A. Barghouty, *Partial cross sections of nucleus-nucleus reactions*, *Astrophys. J.* **501** (1998) 920.
- [81] R. Silberberg, C.H. Tsao and A.F. Barghouty, *Updated Partial Cross Sections of Proton-Nucleus Reactions*, *Astrophys. J.* **501** (1998) 911 [INSPIRE].
- [82] Y. Génolini et al., *Indications for a high-rigidity break in the cosmic-ray diffusion coefficient*, *Phys. Rev. Lett.* **119** (2017) 241101 [arXiv:1706.09812] [INSPIRE].
- [83] PAMELA collaboration, *PAMELA Measurements of Cosmic-ray Proton and Helium Spectra*, *Science* **332** (2011) 69 [arXiv:1103.4055] [INSPIRE].
- [84] H.S. Ahn et al., *Discrepant hardening observed in cosmic-ray elemental spectra*, *Astrophys. J. Lett.* **714** (2010) L89 [arXiv:1004.1123] [INSPIRE].
- [85] A.D. Panov et al., *Elemental Energy Spectra of Cosmic Rays from the Data of the ATIC-2 Experiment*, *Bull. Russ. Acad. Sci. Phys.* **71** (2007) 494 [astro-ph/0612377] [INSPIRE].
- [86] D. Maurin, F. Melot and R. Taillet, *A database of charged cosmic rays*, *Astron. Astrophys.* **569** (2014) A32 [arXiv:1302.5525] [INSPIRE].
- [87] D. Maurin, H. Dembinski, J. Gonzalez, I.C. Maris and F. Melot, *Cosmic-Ray Database Update: Ultra-High Energy, Ultra-Heavy, and Antinuclei Cosmic-Ray Data (CRDB v4.0)*, *Universe* **6** (2020) 102 [arXiv:2005.14663] [INSPIRE].
- [88] C. Pizzolotto et al., *Looking for cosmic ray data? The ASI Cosmic Ray Database*, *PoS ICRC2017* (2018) 227 [INSPIRE].
- [89] M. Korsmeier and A. Cuoco, *Testing the universality of cosmic-ray nuclei from protons to oxygen with AMS-02*, *Phys. Rev. D* **105** (2022) 103033 [arXiv:2112.08381] [INSPIRE].
- [90] J. Chmeleff and et al., *Determination of the ^{10}Be half-life by multicollector ICP-MS and liquid scintillation counting*, *Nucl. Instrum. Meth. B* **268** (2010) 192.
- [91] N.E. Yanasak et al., *Measurement of the Secondary Radionuclides ^{10}Be , ^{26}Al , ^{36}Cl , ^{54}Mn , and ^{14}C and Implications for the Galactic Cosmic-Ray Age*, *Astrophys. J.* **563** (2001) 768.
- [92] M. Garcia-Munoz, G.M. Mason and J.A. Simpson, *The age of the galactic cosmic rays derived from the abundance of ^{10}Be* , *Astrophys. J.* **217** (1977) 859.
- [93] M. Garcia-Munoz, J.A. Simpson and J.P. Wefel, *The Propagation Lifetime of Galactic Cosmic Rays Determined from the Measurement of the Beryllium Isotopes*, in *International Cosmic Ray Conference*, vol. 2 of *International Cosmic Ray Conference*, p. 72, January 1981.
- [94] M.E. Wiedenbeck and D.E. Greiner, *A cosmic-ray age based on the abundance of ^{10}Be* , *Astrophys. J.* **239** (1980) L139.
- [95] T. Hams et al., *Measurement of the abundance of radioactive ^{10}Be and other light isotopes in cosmic radiation up to 2 GeV/nucleon with the balloon-borne instrument ISOMAX*, *Astrophys. J.* **611** (2004) 892 [INSPIRE].
- [96] J.J. Connell, *Galactic Cosmic-Ray Confinement Time: Ulysses High Energy Telescope Measurements of the Secondary Radionuclide ^{10}Be* , *Astrophys. J.* **501** (1998) L59.
- [97] W. Webber, A. Lukasiak and F. McDonald, *Voyager measurements of the charge and isotopic composition of cosmic ray Li, Be, and B nuclei and implications for their production in the galaxy*, *Astrophys. J.* **568** (2002) 210.
- [98] FERMI-LAT collaboration, *Fermi-LAT measurement of the diffuse gamma-ray emission and constraints on the Galactic Dark Matter signal*, *Nucl. Phys. B Proc. Suppl.* **239-240** (2013) 88 [arXiv:1212.6755] [INSPIRE].

- [99] G. Di Bernardo, C. Evoli, D. Gaggero, D. Grasso and L. Maccione, *Cosmic Ray Electrons, Positrons and the Synchrotron emission of the Galaxy: consistent analysis and implications*, *JCAP* **03** (2013) 036 [[arXiv:1210.4546](#)] [[INSPIRE](#)].
- [100] K. Beuermann, G. Kanbach and E. Berkhuijsen, *Radio structure of the galaxy-thick disk and thin disk at 408 mhz*, *Astron. Astrophys.* **153** (1985) 17.
- [101] E. Orlando and A. Strong, *Galactic synchrotron emission with cosmic ray propagation models*, *Mon. Not. Roy. Astron. Soc.* **436** (2013) 2127 [[arXiv:1309.2947](#)] [[INSPIRE](#)].
- [102] F. Spanier and R. Schlickeiser, *Damping and wave energy dissipation in the interstellar medium. II. Fast magnetosonic waves*, *Astron. Astrophys.* **436** (2005) 9.
- [103] S.R. Spangler, A.H. Savage and S. Redfield, *Ion-Neutral Collisions in the Interstellar Medium: Wave Damping and Elimination of Collisionless Processes*, *AIP Conf. Proc.* **1366** (2011) 97 [[arXiv:1012.4121](#)] [[INSPIRE](#)].
- [104] I. Lerche and R. Schlickeiser, *Linear Landau damping and wave energy dissipation in the interstellar medium*, *Astron. Astrophys.* **366** (2001) 1008.
- [105] L.O. Drury and A.W. Strong, *Power requirements for cosmic ray propagation models involving diffusive reacceleration; estimates and implications for the damping of interstellar turbulence*, *Astron. Astrophys.* **597** (2017) A117 [[arXiv:1608.04227](#)] [[INSPIRE](#)].
- [106] V.S. Ptuskin, I.V. Moskalenko, F.C. Jones, A.W. Strong and V.N. Zirakashvili, *Dissipation of magnetohydrodynamic waves on energetic particles: impact on interstellar turbulence and cosmic ray transport*, *Astrophys. J.* **642** (2006) 902 [[astro-ph/0510335](#)] [[INSPIRE](#)].
- [107] O. Fornieri, D. Gaggero, S.S. Cerri, P. De la Torre Luque and S. Gabici, *The theory of cosmic-ray scattering on pre-existing MHD modes meets data*, *Mon. Not. Roy. Astron. Soc.* **502** (2021) 5821 [[arXiv:2011.09197](#)] [[INSPIRE](#)].
- [108] FERMI-LAT collaboration, *Fermi-LAT Observations of the Diffuse Gamma-Ray Emission: Implications for Cosmic Rays and the Interstellar Medium*, *Astrophys. J.* **750** (2012) 3 [[arXiv:1202.4039](#)] [[INSPIRE](#)].
- [109] FERMI-LAT collaboration, *Development of the Model of Galactic Interstellar Emission for Standard Point-Source Analysis of Fermi Large Area Telescope Data*, *Astrophys. J. Suppl.* **223** (2016) 26 [[arXiv:1602.07246](#)] [[INSPIRE](#)].
- [110] E. Amato, *The theory of pulsar wind nebulae*, *Int. J. Mod. Phys. Conf. Ser.* **28** (2014) 1460160 [[arXiv:1312.5945](#)] [[INSPIRE](#)].
- [111] P.D. Serpico, *On the possible causes of a rise with energy of the cosmic ray positron fraction*, *Phys. Rev. D* **79** (2009) 021302 [[arXiv:0810.4846](#)] [[INSPIRE](#)].
- [112] D. Gaggero, D. Grasso, A. Marinelli, A. Urbano and M. Valli, *The gamma-ray and neutrino sky: A consistent picture of Fermi-LAT, Milagro, and IceCube results*, *Astrophys. J. Lett.* **815** (2015) L25 [[arXiv:1504.00227](#)] [[INSPIRE](#)].
- [113] I.V. Moskalenko, A.W. Strong, J.F. Ormes and M.S. Potgieter, *Secondary anti-protons and propagation of cosmic rays in the galaxy and heliosphere*, *Astrophys. J.* **565** (2002) 280 [[astro-ph/0106567](#)] [[INSPIRE](#)].
- [114] K.M. Ferriere, *The interstellar environment of our galaxy*, *Rev. Mod. Phys.* **73** (2001) 1031 [[astro-ph/0106359](#)] [[INSPIRE](#)].
- [115] FERMI-LAT collaboration, *High Energy Gamma-Ray Emission from the Loop I region*, [arXiv:0912.3478](#) [[INSPIRE](#)].
- [116] FERMI-LAT collaboration, *The Spectrum and Morphology of the Fermi Bubbles*, *Astrophys. J.* **793** (2014) 64 [[arXiv:1407.7905](#)] [[INSPIRE](#)].

- [117] FERMI-LAT collaboration, *Local interstellar cosmic-ray spectra derived from gamma-ray emissivities*, [arXiv:1507.05006](#) [INSPIRE].
- [118] O. Fornieri, D. Gaggero and D. Grasso, *Features in cosmic-ray lepton data unveil the properties of nearby cosmic accelerators*, *JCAP* **02** (2020) 009 [[arXiv:1907.03696](#)] [INSPIRE].
- [119] A. De Angelis et al., *Science with e-astrogam: A space mission for mev-gev gamma-ray astrophysics*, *JHEAp* **19** (2018) 1.
- [120] C.F. McKee, A. Parravano and D.J. Hollenbach, *Stars, Gas, and Dark Matter in the Solar Neighborhood*, *Astrophys. J.* **814** (2015) 13 [[arXiv:1509.05334](#)] [INSPIRE].
- [121] M.S. Pshirkov, P.G. Tinyakov, P.P. Kronberg and K.J. Newton-McGee, *Deriving global structure of the Galactic Magnetic Field from Faraday Rotation Measures of extragalactic sources*, *Astrophys. J.* **738** (2011) 192 [[arXiv:1103.0814](#)] [INSPIRE].
- [122] T.A. Porter, I.V. Moskalenko, A.W. Strong, E. Orlando and L. Bouchet, *Inverse Compton Origin of the Hard X-Ray and Soft Gamma-Ray Emission from the Galactic Ridge*, *Astrophys. J.* **682** (2008) 400 [[arXiv:0804.1774](#)] [INSPIRE].
- [123] E.C. Stone, A.C. Cummings, F.B. McDonald, B.C. Heikkila, N. Lal and W.R. Webber, *Voyager 1 observes low-energy galactic cosmic rays in a region depleted of heliospheric ions*, *Science* **341** (2013) 150.
- [124] FERMI-LAT collaboration, *Fermi LAT observations of cosmic-ray electrons from 7 GeV to 1 TeV*, *Phys. Rev. D* **82** (2010) 092004 [[arXiv:1008.3999](#)] [INSPIRE].
- [125] DAMPE collaboration, *Direct detection of a break in the teraelectronvolt cosmic-ray spectrum of electrons and positrons*, *Nature* **552** (2017) 63 [[arXiv:1711.10981](#)] [INSPIRE].
- [126] O. Adriani et al., *Extended Measurement of the Cosmic-Ray Electron and Positron Spectrum from 11 GeV to 4.8 TeV with the Calorimetric Electron Telescope on the International Space Station*, *Phys. Rev. Lett.* **120** (2018) 261102 [[arXiv:1806.09728](#)] [INSPIRE].
- [127] AMS collaboration, *Electron and Positron Fluxes in Primary Cosmic Rays Measured with the Alpha Magnetic Spectrometer on the International Space Station*, *Phys. Rev. Lett.* **113** (2014) 121102 [INSPIRE].